Monthly Notices of the ROYAL ASTRONOMICAL SOCIETY
MNRAS **490,** 3287–3308 (2019) doi:10.1093/mnras/stz2606

Optical, *J* and *K* light curves of XTE J1118+480 = KV UMa: the mass of the black hole and the spectrum of the non-stellar component

A. M. Cherepashchuk,[1⋆] N. A. Katysheva,[1⋆] T. S. Khruzina,[1] S. Yu. Shugarov,[1,2] A. M. Tatarnikov[1] and A. I. Bogomazov[1⋆]

[1] *M. V. Lomonosov Moscow State University, P. K. Sternberg Astronomical Institute, 119991, Universitetkij prospect 13, Moscow, Russia*
[2] *Astronomical Institute, Slovak Academy of Sciences, 05960, Tatranská Lomnica, Slovakia*

Accepted 2019 September 11. Received 2019 August 17; in original form 2019 June 10

ABSTRACT

Optical, J and K photometric observations of the KV UMa black hole X-ray nova in its quiescent state obtained in 2017–2018 are presented. A significant flickering within light curves was not detected, although the average brightness of the system faded by $\approx 0.1^m$ over 350 d. Changes in the average brightness were not accompanied with an increase or decrease in the flickering. From the modelling of five light curves the inclination of the KV UMa orbit and the black hole mass were obtained: $i = 74 \pm 4^{\circ}$, $M_{\rm BH} = (7.06\text{–}7.24)\,{\rm M}_{\odot}$, depending on the mass ratio used. The non-stellar component of the spectrum in the range $\lambda = 6400\text{–}22\,000$ Å can be fitted by a power law $F_\lambda \sim \lambda^\alpha$, $\alpha \approx -1.8$. The accretion disc orientation angle changed from one epoch to another. The model with spots on the star was inadequate. Evolutionary calculations using the SCENARIO MACHINE code were performed for low-mass X-ray binaries, with a recently discovered anomalously rapid decrease of the orbital period taken into account. We show that the observed decrease can be consistent with the magnetic stellar wind of the optical companion, whose magnetic field was increased during the common-envelope stage. Several constraints on evolutionary scenario parameters were developed.

Key words: binaries: close – stars: black holes – stars: individual: KV UMa.

1 INRODUCTION

X-ray novae are the main source of information about the masses of black holes in X-ray binary systems (see e.g. Casares & Jonker 2014 and references therein). They are low-mass X-ray binaries, where the low-mass K–M optical star fills its Roche lobe and its matter outflows on to the relativistic object (a neutron star or a black hole). An accretion disc forms around the compact star. Most of the time X-ray novae are in quiescence, when their X-ray luminosity is small ($\lesssim 10^{31}$–10^{33} erg s^{-1}). Instabilities in the accretion disc lead to an increase in the disc's matter turbulence and to an increase in the accretion rate. This leads to an outburst of the X-ray radiation with a duration of about a month. The maximum X-ray luminosity during the outburst is about 10^{36}–10^{38} erg s^{-1}. The X-ray outburst is accompanied by an optical outburst due to the heating of the disc and the star by the powerful X-ray radiation. In quiescence the system's spectrum contains absorption lines of the optical star. The main cause of the optical variability of X-ray novae in quiescence is the ellipticity effect (Lyutyi, Syunyaev & Cherepashchuk 1973). The optical radiation of the accretion disc and of the region of interaction between the gas stream and the disc also makes an important contribution to the system's optical luminosity in low-mass X-ray binaries. A significant number of X-ray novae contain a black hole as a relativistic object.

Recently it was realized that even in quiescence there are non-stationary processes in X-ray novae with black holes. These are manifested in the fact that some X-ray novae in quiescence show passive and active states of optical variability (Cantrell et al. 2008, 2010; Cherepashchuk et al. 2019). In the passive state the amplitude of the irregular variability (flickering) is relatively low; the orbital light curve has a regular shape. In the active state the average brightness of the system grows by several tenths of stellar magnitude; the amplitude of the flickering sharply grows. The orbital light curve at this state has irregular changes.

In addition, in the black hole X-ray novae A0620-00 and Swift 71354.2-0933, linear polarization of the IR radiation was found; this can indicate the synchrotron radiation of relativistic jets (Russell et al. 2016). Also in these systems an anomalously fast decrease in the orbital period was found (González Hernández, Rebolo & Casares 2012, 2014; González Hernández et al. 2017), spectroscopic effects of the precession of the elliptical accretion disc (Shahbaz et al. 2004; Zurita et al. 2016) were detected, and there were observed spectroscopic traces of chromospheric activity of the donor

⋆ E-mail: cherepashchuk@gmail.com (AMC); natkat2006@mail.ru (NAK); a78b@yandex.ru (AIB)

star (Casares et al. 1997; Torres et al. 2002; Zurita, Casares & Shahbaz 2003; González Hernández & Casares 2010; Zurita et al. 2016).

The X-ray binary XTE J1118+480 = KV UMa belongs to a class of low-mass transient X-ray binary systems with black holes. An X-ray outburst of KV UMa was detected from the RXTE satellite on 2000 March 29 (Remillard et al. 2000). At the same time the optical brightness of the system had grown by $\approx 6^m$ from $V \approx 18.8^m$ in quiescence to $V \approx 12.9^m$ at maximum (Uemura et al. 2000a; Garcia et al. 2000).

The galactic latitude of KV UMa is particularly high: $b = +62^{\circ}$. Along with the distance to the system 1.9 ± 0.4 kpc (Wagner et al. 2001), this corresponds to a significant height over the galactic plane $z = 1.7 \pm 0.4$ kpc. The interstellar absorption to KV UMa is very weak, $E(B - V) = 0.013$–0.017, $A_v = 0.05^m$, which makes the multi-wavelength analysis of this system easier (Shahbaz et al. 2005; Khargharia et al. 2013).

Multi-wavelength observations of KV UMa during outbursts have been conducted by Hynes et al. (2003), Torres et al. (2004). They observed superhumps that indicated the precession of the accretion disc (Cook et al. 2000; Uemura et al. 2000b; Patterson et al. 2000; Dubus et al. 2001).

By the end of 2000 August the KV UMa brightness returned to the value before the outburst ($V \approx 19^m$). Spectroscopic observations during that period of time by Wagner et al. (2001), McClintock et al. (2001b) allowed: (i) the spectral type of the optical star (K7–M0)V to be found, (ii) a reliable radial velocity curve to be obtained, (iii) the orbital period to be calculated, and (iv) the spectroscopic elements of the system to be computed. The KV UMa mass function turned out to be very high, $f_v(M) = 6.1 \pm 0.3\,\mathrm{M}_{\odot}$. The contribution of the optical star radiation to the total flux in the wavelength 5900 Å estimated using spectrophotometry was on average 32 ± 6 per cent.

Torres et al. (2004) showed that the evolution of the KV UMa spectrum in the wavelength range $\lambda = 5800$–6400 Å from the beginning of the outburst decay until quiescence took place due to the change of the contribution of the donor star in the total flux from 35 ± 8 per cent on 2000 December 9 and 2001 January 26 to 60 ± 10 per cent on 2003 January 2–3. This is consistent with data from other authors: 53 ± 7 per cent in 2001 April (Zurita et al. 2002) and 45 ± 10 per cent in 2002 January (McClintock et al. 2003). Khargharia et al. (2013) gave a spectrophotometric estimate of the contribution of the optical star in the H band as 54 ± 27 per cent in 2011 April, i.e. in quiescence.

Doppler tomography of KV UMa was done by Torres et al. (2004), Calvelo et al. (2009), Zurita et al. (2016). Zurita et al. (2016) analysed movements of the H α emission centroid and found that the precession period of the accretion disc was $\approx$52 d. This was in agreement with the precession period of the disc found using the analysis of superhumps in light curves (Cook et al. 2000; Patterson et al. 2000; Uemura et al. 2002; Zurita et al. 2002). Also, a narrow H α emission component was observed. It belonged to the optical star and, according to Zurita et al. (2016), it indicated a chromospheric activity of the donor star.

IR light curves in the J, K bands were obtained in 2003 April and 2004 March by Mikołajewska et al. (2005). In the J band the star had the same brightness in minima, but the maxima were not equal. The non-stellar component contributions in the J, K bands in 2003 April and 2004 March did not exceed 33 per cent and 25 per cent respectively.

The first modelling of the KV UMa optical light curve was done by McClintock et al. (2001a) under the assumption that the contribution of the accretion disc to the total brightness was 66 per cent; the inclination of the system's orbit was computed ($i = 80^{\circ}$). The KV UMa light curve in the R band was observed by Wagner et al. (2001). In the model with an accretion disc around the relativistic object (its contribution was 76 per cent) the inclination of the orbit was $i = 81 \pm 2^{\circ}$. That light curve was interpreted by Khruzina et al. (2005) in the model that included the disc and the region of the interaction between the accretion stream and the disc ('hot line'). The inclination of the orbit was estimated to be $i = 80^{+1}_{-4}{}^{\circ}$.

Gelino et al. (2006) obtained *BVRJHK* light curves of KV UMa in 2003 January. Under the assumption of a negligible contribution of the accretion disc in the IR wavelength (less than 8 per cent; light curves in IR are symmetric with practically equal maxima and minima) they computed the inclination of the orbit $i = 68^{+2.8}_{-2}{}^{\circ}$ and gave an estimate of the black hole mass $M_{\mathrm{BH}} = 8.53\,\mathrm{M}_{\odot} \pm 0.6\,\mathrm{M}_{\odot}$. Khargharia et al. (2013) conducted spectroscopic observations of KV UMa in the range 0.9–2.45 μm and obtained a light curve in the H band. As in the work by Mikołajewska et al. (2005) their H light curve had different maxima and equal minima. Khargharia et al. (2013) considered two models (a model with an accretion disc and a model with a disc and a hotspot on the outer border of the disc) and estimated the orbit's inclination as $68^{\circ} \leq i \leq 79^{\circ}$ and the black hole mass $6.9\,\mathrm{M}_{\odot} \leq M_{\mathrm{BH}} \leq 8.2\,\mathrm{M}_{\odot}$. They emphasized that KV UMa (similar to other X-ray novae in quiescence) demonstrated the presence of continued activity even if the system was in its quiescent state with a very low X-ray luminosity.

We made long-lasting optical, J and K photometric observations of KV UMa in order to find manifestations of such activity and to determine the inclination of the orbit and the black hole mass in the frames of an adequate model of the system. In addition it was planned to reconstruct the non-stellar component spectrum and to attempt to find traces of the precession of the elliptical accretion disc. Also, some evolutionary calculations for low-mass X-ray binaries with black holes were made.

Section 2 describes our observations of KV UMa conducted in 2017–2018 in the infrared and optical ranges, the telescopes and techniques used for them. Section 3 depicts light curves obtained from our observations and compares our curves with previous results of other authors. Section 4 presents a theoretical modelling of the obtained light curves, Section 5 evaluates the model. Section 6 shows the results of the modelling and describes our spectrophotometric conclusions concerning the non-stellar component. Section 7 discusses the model and its applications. The appendix studies the evolution of low-mass X-ray binaries with black holes, paying special attention to the rapid decrease of the orbital period in the closest pairs.

2 OBSERVATIONS

Observations of KV UMa were performed over three seasons in 2017 and 2018 in the optical and infrared spectral ranges. Since the orbital period of the system is short (about 4 h), we tried to cover it completely during the night depending on weather conditions. At that time KV UMa was in quiescence. The observation log is given in Table 1.

For the integral light (marked as 'C') the 180 s exposition was used. In the IR range this was from 30–100 s (see Table 1) depending on weather conditions.

2.1 IR observations

IR observations in the J ($\lambda_{\mathrm{eff}} \approx 1.25\ \mu$m) and K ($\lambda_{\mathrm{eff}} \approx 2.2\ \mu$m) bands of the Mauna Kea Observatories (MKO) photometric system

Table 1. A log of KV UMa observations.

Data	JD-245 0000	Band	Telescope
2017 November 24	8082.622 - .664	*C*	EMT
2017 November 25	8083.458 - .665	*C*	EMT
2017 December 15	8103.411 - .416	*J*, 100 s	CMO
2018 January 16	8135.475 - .541	*J*, 100 s	CMO
2018 January 28	8147.426 - .492	*K*, 30 s	CMO
2018 January 28	8147.431 - .494	*J*, 30 s	CMO
2018 February 7	8157.378 - .632	*J*, 30 s	CMO
2018 February 7	8157.384 - .631	*K*, 30 s	CMO
2018 April 8	8217.313 - .552	*J*, 100 s	CMO
2018 April 17	8226.304 - .400	*K*, 60 s	CMO
2018 April 24	8233.300 - .755	*K*, 60 s	CMO
2018 April 25	8234.409 - .560	*J*, 100 s	CMO
2018 April 26	8235.374 - .554	*J*, 100 s	CMO
2018 June 1	8271.281 - .380	*C*	EMT
2018 June 4	8274.279 - .378	*C*	EMT
2018 June 5	8275.281 - .785	*C*	EMT
2018 June 6	8276.295 - .372	*C*	EMT
2018 June 7	8277.283 - .371	*C*	EMT
2018 June 9	8279.280 - .365	*C*	EMT
2018 November 1	8424.510 - .566	*C*	EMT
2018 November 2	8425.489 - .637	*C*	EMT
2018 November 3	8426.491 - .641	*C*	EMT
2018 November 4	8427.537 - .642	*C*	EMT
2018 November 5	8428.639 - .623	*C*	EMT
2018 November 8	8431.490 - .646	*C*	EMT
2018 November 9	8432.502 - .625	*C*	EMT
2018 November 10	8433.473 - .639	*C*	EMT
2018 November 13	8436.486 - .534	*C*	EMT

were conducted on the newly installed 2.5 m telescope at the Caucasian Mountain Observatory (CMO) of SAI MSU (Sternberg Astronomical Institute, Lomonosov Moscow State University) located in the Karachay-Cherkess Republic (Russian Federation) at an altitude 2112 m above sea level (CMO in Table 1).

Infrared observations in the *J* band were conducted on 2017 December 15, 2018 January 16 and 28, February 7, 8, 25 and April 26 and in the *K* band on 2018 January 28, February 7 and April 17; a short piece of photometric observation was obtained in the *H* band on 2018 January 18. The ASTRONICAM camera-spectrograph (Nadjip et al. 2017) with the Hawaii-2RG detector (2048 × 2048 pixels) was used; in the photometric regime only the central part (1024 × 1024 pixels) of it can be in operation.

2MASS J11181198+4802190 was used as a comparison star for IR observations ('5' in Fig. 1). We attributed the following MKO magnitudes to it: $J = 16.247^m$, $H = 15.624^m$, $K = 15.46^m$.

The average error in IR bands estimated using control stars 4 and 6 (see Fig. 1) was 0.02^m. During the first analysis of data in the *J* band we divided them into two series: from 2017 December 15 to 2018 February 7, and from 2018 April 8–26. The dimension of the first series was 298 points, for the second it was 404 points; as a result of averaging of individual measurements we got 60 and 81 points respectively. It was found that the light curves changed insignificantly during observations, so we used a combined series to create an averaged *J* light curve.

In the *K* band there were obtained 415 points, then five image-averaging tasks were performed to increase the precision. After removing points out of the 3σ level (as for the *J* band), 83 points remained (2017 January 28–2018 April 25). The error in the *K* band is higher than that in the *J* band and is equal to 0.03^m (on average).

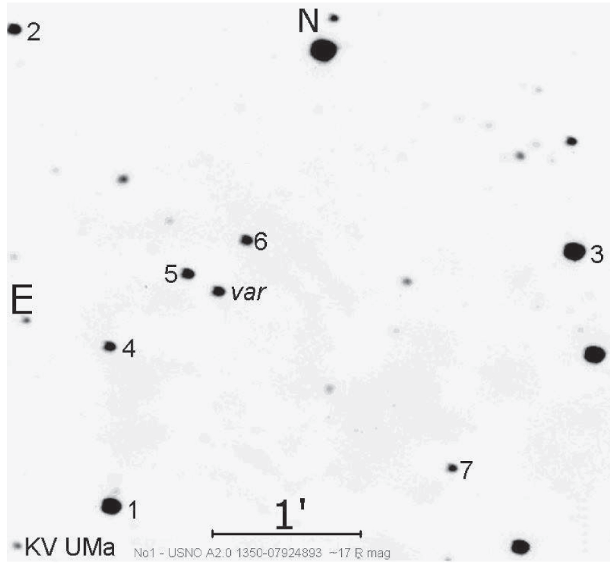

Figure 1. A finding chart for KV UMa surroundings, $4' \times 4'$; 'var' is KV UMa, the north is 'N', the east is 'E'.

2.2 Optical observations

Optical observations were unfiltered and performed in the integral light with the effective wavelength $\lambda_{\mathrm{eff}} \approx 6400$ Å that corresponded to the average wavelength with the bandwidth at half intensity $\lambda =$ 4300–8300 Å (see e.g. Armstrong et al. 2013; Khruzina et al. 2015, where the parameters of this band were discussed) using the 1.25 m V. P. Engelgardt Mirror Telescope at the Crimea Astronomical Station of M. V. Lomonosov Moscow State Univeristy (EMT in Table 1) with the CCD camera VersArray-1300. The object was observed on 2017 November 24, 25, 2018 June 1, 2, 4–7, 9 and November 1–5, 8–10, 13.

To process the optical data the USNO A2.0 1350−0792893 reference star ('1' in Fig. 1) was used with following stellar magnitudes: $B = 19.144^m$, $V = 17.758^m$, $R_C = 16.895^m$, $I_C = 16.352^m$ (according to observational data in 2018 November), where R_C and I_C are in the Cousins system. Also we conducted quasi-synchronous observations in integral light (C_m) and in the R_C band. A comparison of stellar magnitudes $C_m = 18.821^m$ and $R_C = 18.820^m$ showed that it was possible to use the R_C value to make a light curve.

Bias and flat-field corrections were made for all *C*, *J*, and *K* images.

3 LIGHT CURVES

To compute the light curves we used the following ephemeris:

$$\mathrm{Min}\ (\varphi = 0.0) = T_0 + P_{\mathrm{orb}} \times E, \tag{1}$$

where T_0 = HJD 245 5676.6017 is the initial epoch, $P_{\mathrm{orb}} = 0.169\,9337 \pm 0.000\,0002$ d and *E* is the number of orbital cycles after T_0.

The $\varphi = 0.0$ phase corresponds to the upper conjunction of the relativistic object (the optical star is in front of it; González Hernández et al. 2014).

Fig. 2(a) shows photometric measurements in white convolved with the orbital period (*C* is the difference of stellar magnitudes with respect to the main comparison star as $C = C_{\mathrm{var}} - C_{\mathrm{control}}$), and Fig. 2(b) is the same for the *J*, *K* bands. Our measurements

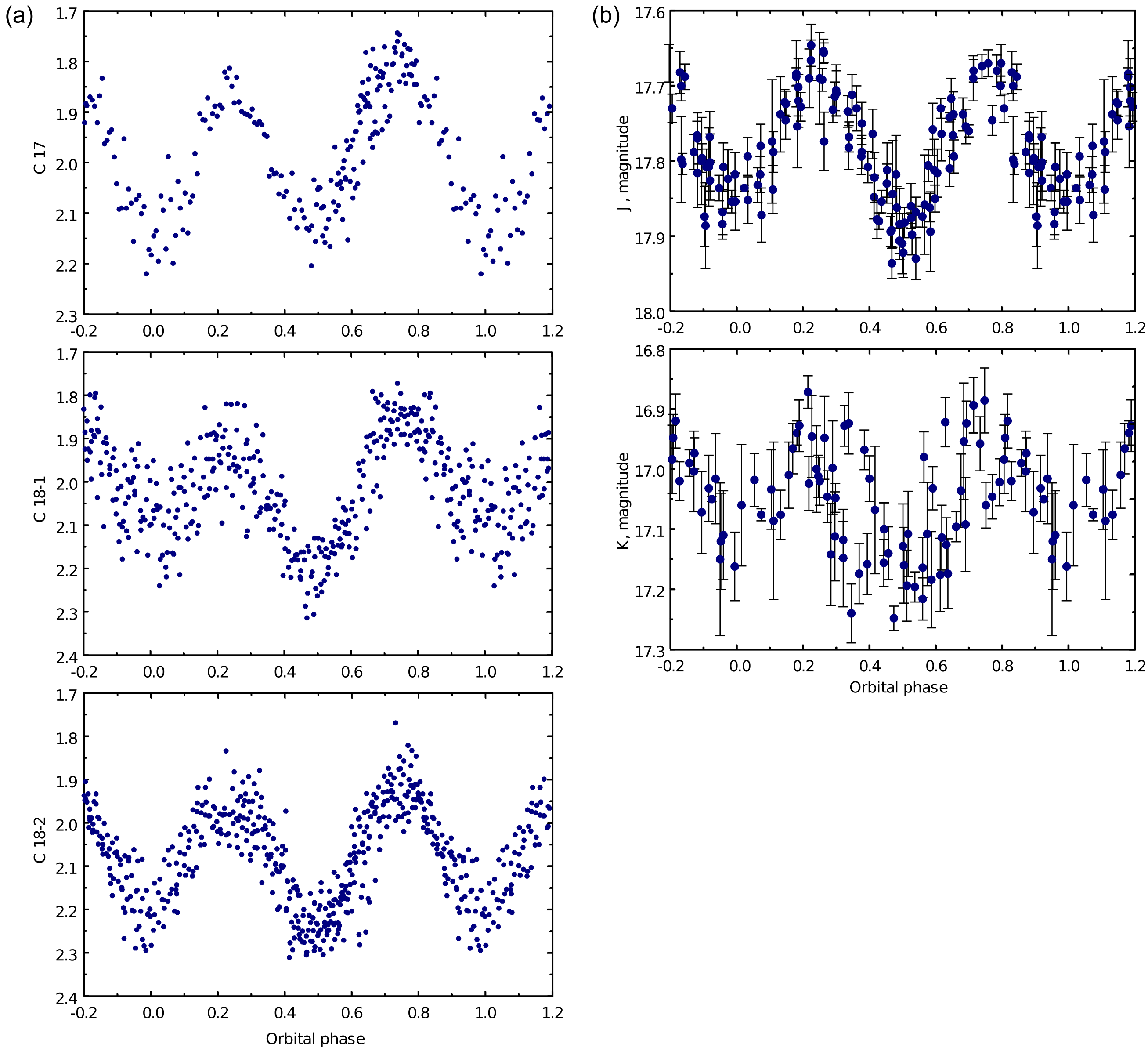

Figure 2. (a) Average phase optical light curves of KV UMa obtained during the season (see Table 1). The data were convolved using ephemeris 1. (b) Average IR phase light curves of KV UMa obtained during the season (see Table 1). The data were convolved using ephemeris 1.

are shown in integral light for three seasons in 2017 November (JD245 8082–8083), 2018 June (JD245 8271–8279), 2018 November (JD245 8424–8436), in J, K from the end of 2017 December to 2018 April (JD245 8103–8235).

We did not detect the presence of a considerable flickering within the light curves during three observational seasons (about 350 d depending on the wavelength band); see Table 1. The scatter of individual points can be basically explained by errors of measurements estimated using control stars. The average optical brightness of the system changed significantly (see Fig. 3, light curves obtained in 2017 November, 2018 June, and 2018 November) and the system monotonically faded. This is clearly seen in the composite image (Fig. 3) that shows three average phase curves in the integral light in 2017 November (C17), 2018 June and November (C18-1 and C18-2). The number of images obtained in 2017 November was $N = 220$ and the average stellar magnitude of the system $C = 18.86 \pm 0.01$; in 2018 June $N = 327$, $C =$

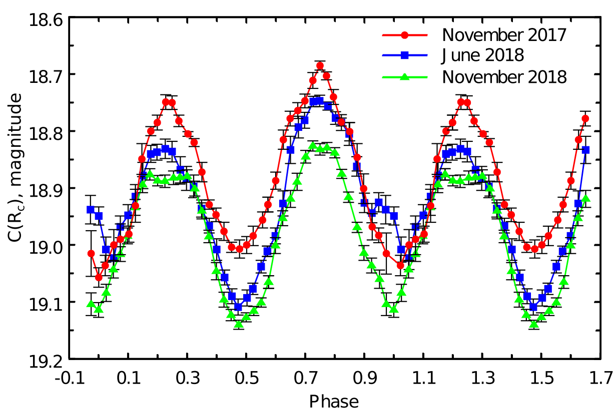

Figure 3. Average phase curves of KV UMa in the integral light. About ~1000 individual measurements were used. Errors of individual observations were 0.025^m–0.030^m (on average).

18.91 ± 0.01; and in 2018 November $N = 434$, $C = 18.97 \pm 0.01$. The averaged integral stellar magnitude in 2017 November–2018 June was $C = 18.929 \pm 0.004$.

Fig. 3 shows that the light curves in integral light changed during the year: the secondary maxima became lower by about 0.15^m, and the shape of the primary minimum in 2018 November also changed (it became flat). The optical light curves showed considerable inequality of maxima with the same character (but expressed less) as the IR light curves obtained by Mikołajewska et al. (2005), Khargharia et al. (2013). The optical light curves also showed an inequality in minima that changed its sign in different epochs: in 2017 November the system was brighter in the secondary minimum than in the primary minimum ($\varphi = 0.0$). In 2018 June and November the situation was opposite: the system was brighter in the primary minimum than in the secondary minimum (see Fig. 3). In IR (Fig. 2b) the inequality of maxima had the opposite sign in comparison with the optical range: the maximum at the phase $\varphi = 0.25$ was higher that at the phase $\varphi = 0.75$.

A comparison of our IR data with data by Mikołajewska et al. (2005) obtained in 2003 April and 2004 March showed that our light curve in the J band had different ratios of maxima (the maximum at the phase 0.25 was higher than at the phase 0.75). In addition, the average brightness and the colour index of the system were $J = 18.03^m \pm 0.04^m$, $J - K = 1.11^m \pm 0.2^m$ in the paper by Mikołajewska et al. (2005); in our case they were $J = 17.79^m \pm 0.02^m$, $J - K = 0.73^m \pm 0.04^m$, i.e. the system became brighter in the J band by 0.23^m and bluer. The amplitude of the orbital variability in the J band in our case dropped to $\Delta J \approx 0.23^m$ in comparison to a J light curve by Mikołajewska et al. (2005) ($\Delta J \approx 0.35^m$). These differences are most likely connected with the variability of the contribution of the non-stellar component to the total brightness of the system (the accretion disc with the region of interaction between the disc and the gas stream). Despite the different photometric systems, the difference in the brightness in 2003–2004 and 2017–2018 should be connected with the physical variability.

It should be emphasized that in the optical light and in the IR range the considerable growth of the average brightness of the system was not accompanied by an increase in flickering. In this feature KV UMa differed from the low-mass X-ray nova A0620-00 (see e.g. Shugarov et al. 2016; Cherepashchuk et al. 2019).

4 MODELLING OF LIGHT CURVES

Average standard light curves were used for the modelling. The orbital period was divided by phase intervals; in each interval a mean of individual stellar magnitudes was computed along with its mean square error.

Figs 4(a) and (b) show average optical and IR light curves (dots) and optimal theoretical light curves (lines) that correspond to final optimal values of parameters (see Tables 2a and b) for two values of the mass ratio $q = M_{\rm BH}/M_v$, where $M_{\rm BH}$ and M_v are the masses of the black hole and the optical star respectively.

For the modelling we used a model of an interacting binary system. The model has already been successfully applied to the analysis of light curves of cataclysmic binary systems (see e.g. Khruzina et al. 2001, 2003a,b; a detailed description was done by Khruzina 2011) along with X-ray binary systems (Khruzina et al. 2005; Cherepashchuk et al. 2019). In this case the standard method to synthesize light curves was used (Wilson & Devinney 1971). The optical star fills its Roche lobe. Gravitational darkening and limb darkening were taken into account (a linear limb-darkening law). An elliptical accretion disc was in the system; a relativistic companion was in one of its focuses. Near the outer border of the disc there was a region of an interaction of a gas stream (a hot line and a hotspot). The hot line was located along the gas stream; the hotspot was located on the outer border of the disc. Heating of the hot line arises due to the lateral collision of the matter of the stream with the rotating matter of the halo around the disc. The matter heated in the corresponding shock waves cooled, joined the outer border of the disc and formed the hotspot. This feature means that our model differs from the classical model with a hotspot in which the spot on the outer border of the disc is heated due to the frontal collision of the stream and the disc. Our model with the hot line and the hotspot satisfies the results of three-dimensional hydrodynamical calculations by Bisikalo (2005), Lukin et al. (2017), who showed that the interaction of the stream with the rotating disc in the frames of a 3D model occurs in a more complicated way than in the classical model of the hotspot.

It is necessary to note that it is very difficult to distinguish the classical model with the hotspot from our model with the interaction region using Doppler tomography, because the widely used method of using maximum entropy to solve ill posed problems allows a stable approximate solution with a minimal tiny structure to be found. The method of maximum entropy (see e.g. Tikhonov et al. 1983; Marsh & Horne 1988) gives smoothed results.

In general form our model can be described using 20 parameters; they can be found if eclipses exist in the cataclysmic binary. In KV UMa eclipses are not observed; therefore we are restricted to a group of parameters with limited values and fixed values of other parameters. The calculation technique can be found in our previous work (Cherepashchuk et al. 2019).

Two values of component mass ratio were used: $q = M_{\rm BH}/M_v = 37$ (González Hernández et al. 2012) and $q = 73$ (Petrov, Antokhina & Cherepashchuk 2017); they were estimated using the rotational broadening of line profiles in the donor star spectrum. This allowed us to test the sensitivity of the problem to the change of q. The temperature of the optical K7V star was fixed as $T_2 = 4120$ K. Fluxes from elementary areas on the star, on the disc and within the interaction region were computed using Planck's law. The ranges of permitted values of other parameters were close to the ranges used for V616 Mon by Cherepashchuk et al. (2019). As a result, in our calculation there remained 11 free parameters: i, R_d/ξ (ξ is the distance between the inner Lagrange point L1 and the black hole), the disc eccentricity e, the azimuth of the periastron of the disc α_e, parameters T_{in} and α_g that characterize the distribution of the temperature in the disc,

$$T(r) = T_{in}\left(\frac{R_1}{r}\right)^{\alpha_g},$$

where $R_1 = 0.0003a_0$ (a_0 is the radius of the relative orbit), a_v/a_0, b_v/a_0 (the semi-minor and semi-major axes of the ellipsoid that fits the hot line in units of a_0), $T^{(1)}_{max}$, $T^{(2)}_{max}$ (the maximum temperatures on the 'front' (windward) side and the 'far' (leeward) side of the hot line with respect to the direction of the disc rotation), and $R_{\rm sp}/a_0$ (the semi-major axis of the hotspot ellipse in units of a_0). The values of e and α_e were not fixed to let to see the dynamics of the changes of these parameters with time. The solution of the inverse problem was conducted using iteration over the parameter i.

For every fixed value of i the minimization of the residual functional over all other 10 parameters was realized. We call here the weighted sum of squares of differences between the observed light curve and the theoretical one the 'residual functional'. The

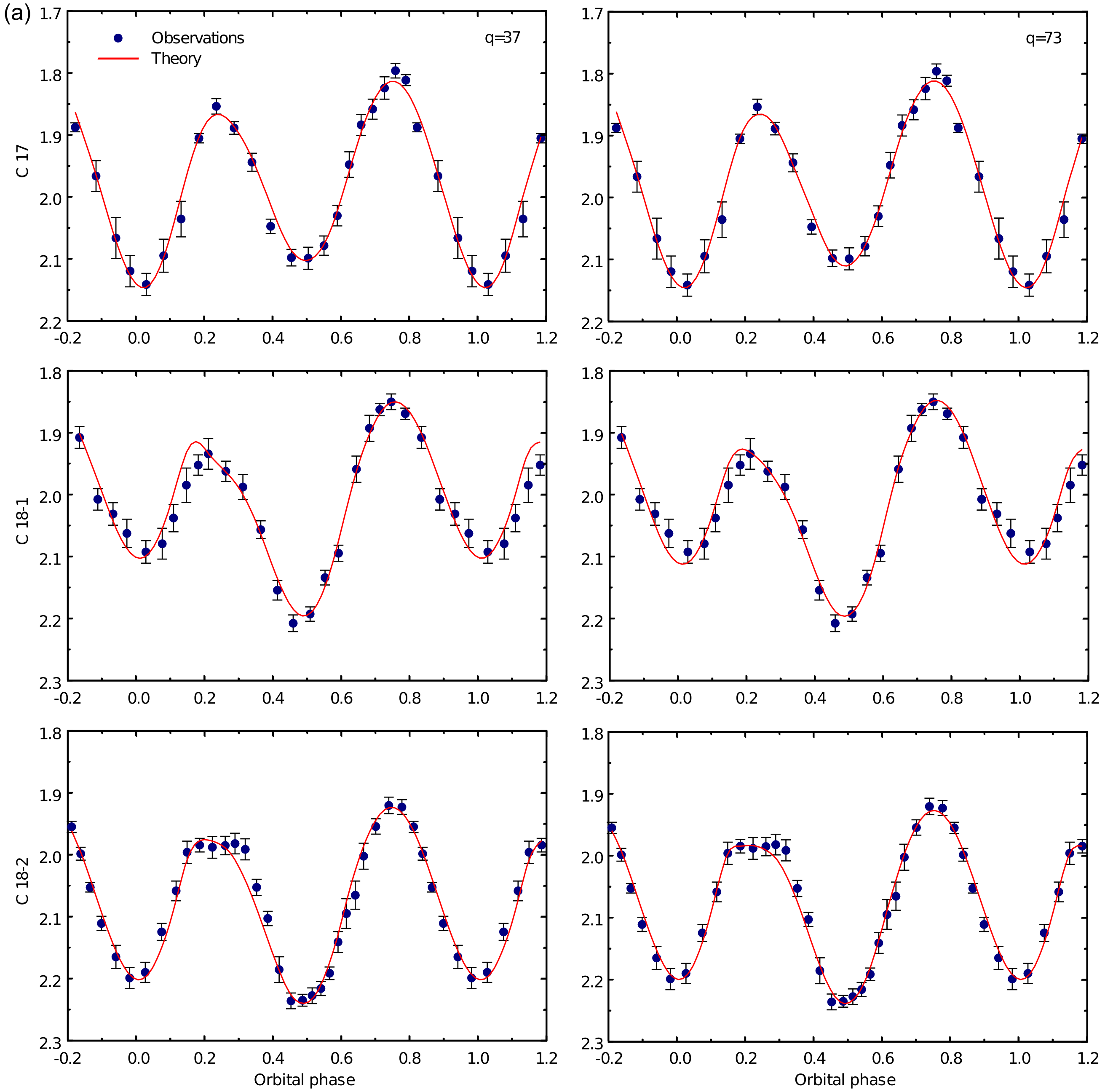

Figure 4. (a) Average light curves of KV UMa and optimal theoretical light curves in the integral light for parameters from Tables 2a and b; two values of the mass ratio $q = M_{\rm BH}/M_v = 37$ and 73 were applied. (b) Average light curves of KV UMa and optimal theoretical light curves in IR for parameters from Tables 2a and b; two values of the mass ratio $q = M_{\rm BH}/M_v = 37$ and 73 were applied.

Nelder–Mead method was used to find the minimum of the residuals (Himmelblau 1972).

5 AN ADEQUACY TEST FOR THE MODEL

To test the adequacy of the model (including estimations concerning contributions of different radiating structures) let us consider our average optical light curve obtained in 2017 November. The adequacy of our model for other epochs was studied too and it is illustrated in Figs 8(a) and (b).

Fig. 5 shows curves of residuals as functions of the orbital inclination i with minimal values of residuals over all other parameters in models of the system. For each i value there is a definite corresponding average value of the non-stellar component luminosity (the disc plus the hotspot plus the hot line), which was determined by the solution of the inverse problem. In Fig. 5 there is a model of the system ($\varphi = 0.695$) that includes the donor star, the disc with the hotspot, and the hot line for optimal values of parameters ($C17$ curve) and $i = 74°$. The dashed line cuts the critical value of $\chi^2 = 24.7$ within a significance level of 1 per cent for the degree of freedom $n - m = 11$ (in the model 'ell+disc+HS+HL', $n = 22$ is the number of points in the light curve, $m = 11$ is the number of parameters for the minimization).

It can be seen that, for the tidally deformed optical star only (see the paper by Lyutyi et al. 1973 for the ellipticity effect) without

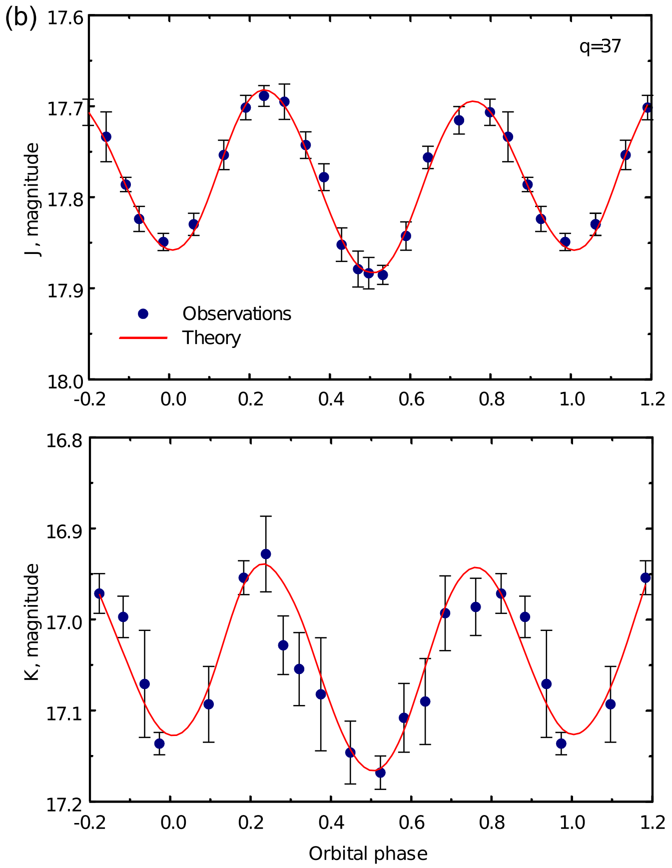

Figure 4. – *continued*

Table 2a. The solution of the inverse problem of interpretation of optical and IR light curves for $q = M_{BH}/M_v = 37$.

Parameters	*C17*	*C18-1*	*C18-2*	*J*	*K*
JD 245 0000+	8082–8083	8271–8279	8424–8436	8103–8235	8147–8234
N	196	327	434	121	83
i, °	74	73	77	68	76
			Disc with hotspot		
R_d, ξ	0.394 ± 0.002	0.398 ± 0.002	0.401 ± 0.002	0.385 ± 0.007	0.366 ± 0.009
a, a_0	0.310 ± 0.002	0.315 ± 0.004	0.317 ± 0.002	0.304 ± 0.006	0.289 ± 0.009
e	0.025 ± 0.004	0.019 ± 0.004	0.022 ± 0.003	0.025 ± 0.009	0.03 ± 0.01
α_e, °	125 ± 2	95 ± 2	145 ± 15	125 ± 7	125 ± 25
T_{in}, K	139 010 ± 575	122 760 ± 210	125 780 ± 370	114 470 ± 265	106 775 ± 635
α_g	0.692 ± 0.002	0.660 ± 0.001	0.657 ± 0.001	0.622 ± 0.001	0.605 ± 0.001
R_{sp}, a_0	0.24 ± 0.03	0.28 ± 0.03	0.25 ± 0.05	0.13 ± 0.03	0.09 ± 0.02
$0.5\beta_d$, °	1.66 ± 0.05	2.0 ± 0.1	1.6 ± 0.1	2.2 ± 0.1	2.7 ± 0.2
			Hot line		
a_v, a_0	0.035 ± 0.001	0.032 ± 0.001	0.032 ± 0.001	0.029 ± 0.001	0.027 ± 0.003
b_v, a_0	0.257 ± 0.002	0.215 ± 0.002	0.233 ± 0.001	0.261 ± 0.003	0.275 ± 0.009
$T_{ww,\,\max}$, K	12 370 ± 305	16 740 ± 250	14 935 ± 500	18 715 ± 500	22 090 ± 995
$T_{lw,\,\max}$, K	10 060 ± 55	12 560 ± 40	11 410 ± 70	13 260 ± 100	14 775 ± 450
F_d/F_{full}	0.246 ± 0.003	0.312 ± 0.003	0.277 ± 0.002	0.435 ± 0.003	0.339 ± 0.001
F_{HL}/F_{full}	0.136 ± 0.009	0.09 ± 0.01	0.073 ± 0.008	0.078 ± 0.005	0.061 ± 0.007
$(F_d + F_{HL})/F_{full}$	0.382 ± 0.010	0.40 ± 0.01	0.350 ± 0.008	0.513 ± 0.005	0.401 ± 0.007
n	22	23	30	19	16
χ^2; χ^2_{crit}	30.2; 24.7	28.4; 26.2	42.4; 36.2	6.19; 20.1	14.4; 15.1

Table 2b. The solution of the inverse problem of interpretation of optical and IR light curves for $q = M_{BH}/M_V = 73$.

Parameters	$C17$	$C18$-1	$C18$-2	J	K
JD 245 0000+	8082–8083	8271–8279	8424–8436	8103–8235	8147–8234
N	196	327	434	121	83
i, °	74	68	78	72	79
			Disc with hotspot		
R_d, ξ	0.398 ± 0.002	0.403 ± 0.002	0.367 ± 0.002	0.379 ± 0.002	0.362 ± 0.006
a, a_0	0.328 ± 0.001	0.333 ± 0.002	0.303 ± 0.001	0.312 ± 0.001	0.298 ± 0.005
e	0.025 ± 0.001	0.021 ± 0.004	0.022 ± 0.004	0.025 ± 0.002	0.025 ± 0.007
α_e, °	125 ± 2	90 ± 18	146 ± 5	125 ± 1	125 ± 30
T_{in}, K	140 075 ± 595	129 050 ± 495	104 000 ± 220	110 295 ± 265	120 070 ± 955
α_g	0.721 ± 0.001	0.716 ± 0.001	0.624 ± 0.001	0.613 ± 0.001	0.593 ± 0.002
R_{sp}, a_0	0.27 ± 0.03	0.22 ± 0.03	0.19 ± 0.05	0.08 ± 0.01	0.10 ± 0.04
$0.5\beta_d$, °	1.25 ± 0.01	1.7 ± 0.1	1.6 ± 0.1	1.8 ± 0.1	2.8 ± 0.1
			Hot line		
a_v, a_0	0.038 ± 0.001	0.037 ± 0.001	0.016 ± 0.001	0.0294 ± 0.0001	0.028 ± 0.003
b_v, a_0	0.265 ± 0.001	0.236 ± 0.001	0.184 ± 0.001	0.280 ± 0.002	0.298 ± 0.003
$T_{ww,\,\max}$, K	12 130 ± 220	13 055 ± 340	14 125 ± 935	16 365 ± 450	22 725 ± 615
$T_{lw,\,\max}$, K	5285 ± 35	10 410 ± 45	10 325 ± 95	11 890 ± 100	15 350 ± 305
F_d/F_{full}	0.215 ± 0.004	0.243 ± 0.003	0.379 ± 0.001	0.497 ± 0.005	0.475 ± 0.002
F_{HL}/F_{full}	0.179 ± 0.009	0.152 ± 0.013	0.027 ± 0.005	0.083 ± 0.006	0.085 ± 0.011
$(F_d + F_{HL})/F_{full}$	0.394 ± 0.011	0.395 ± 0.013	0.406 ± 0.005	0.580 ± 0.006	0.560 ± 0.012
n	22	23	30	19	16
χ^2; χ^2_{crit}	26.5; 24.7	20.4; 26.2	21.6; 36.2	6.95; 20.1	11.4; 15.1

Note. Comments to Tables 2a and b: Parameters were obtained using the following fixed values: $T_2 = 4120$ K, $R_2 = 0.144a_0$, $\xi = 0.8077a_0$, a_0 is the distance between centres of masses of components, $0.5\beta_d$ is the semi-thickness of the outer border of the disc (in degrees), a, e, α_e are the major semi-axis, the eccentricity, and the azimuth of the periastron of the disc respectively, R_2, ξ, a are computed while solving the problem; $\chi^2_{crit} = \chi^2_{n-m,0.01}$ is the critical value of χ^2 for the significance level 1 per cent, n, m are the quantity of average dots in the light curve and the number of variables ($m = 11$) respectively. $(F_d + F_{HL})/F_{full}$, F_d/F_{full}, and F_{HL}/F_{full} are relative contributions of different non-stellar radiating elements to the total system's flux averaged over the orbital period, the disc plus the hot line, the disc only, the hot line only, respectively. Tables 2a and 2b also contain formal estimations of the errors of parameters (except the orbit's inclination i) that correspond to a 10 per cent increase of the χ^2 minimal value.

the disc, the hotspot or the hot line, the corresponding curve of residuals has a clear minimum around $i \approx 55°$. However, the minimal value of the residual ($\chi^2_{min} = 122$) is more than three times higher than the critical value $\chi^2_{n-m,0.01} = 38.9$ for this model ($m = 1$). So, the 'pure' ellipsoidal model is surely rejected. If we take into account the accretion disc (without the hotspot or the hot line) along with the donor star, the value of the residual changes purely. This means that this model is also rejected: the minimum in the residual curve becomes wide and flat, because the ellipticity effect can be compensated with the change in disc luminosity (see Fig. 6). The spectrophotometric estimate of the non-stellar component allows us to choose a point inside the flat minimum corresponding to the optimal value of i. The fact that both described models (the ellipsoidal star alone and the ellipsoidal star plus the accretion disc around the black hole) are strongly inadequate for the observations is connected with a significant inequality of maxima in quadratures of the light curve (see Fig. 7) that cannot be described in these models.

In the model with the donor star, the disc and the hotspot on the outer border of the disc, the minimal value of the residual drops twice ($\chi^2_{min} = 56.4$, $\chi^2_{n-m,0.01} = 34.8$, $m = 4$), but it is still significantly higher than the critical value χ^2, i.e. this model is also surely rejected.

The residual curve in this case also has a wide and flat minimum ($i = 58$–$79°$), and to find i it is necessary to independently know the non-stellar component luminosity.

In the model with the donor star and with the disc with the hotspot and the hot line, the minimal value of the residual ($\chi^2_{min} = 30.2$, $\chi^2_{n-m,0.01} = 24.7$, $m = 11$) is ≈15 per cent higher than the critical value $\chi^2 \approx 24.7$ within the confidence level $\alpha = 0.01$ and it is lower than the critical value for $\alpha = 0.001$ ($\chi^2_{12,0.001} = 32.9$). So, in this case there is a more or less good basis to accept the model. The minimum of residuals determines the optimal value of $i = 74°$; the corresponding average luminosity of the non-stellar component is equal to 0.38 of the total flux from the system and the last theoretical value can be controlled with a spectrophotometric estimate of this luminosity. In addition, the luminosities of both components (the disc plus the hotspot and the hot line) can be found. As follows from Fig. 7, in this case it is possible to make a good description for the amplitude of the light curve and for the inequality of brightness maxima in quadratures.

So, with some reservations, it is possible to accept that the model 'star plus accretion disc with hotspot and hot line' is adequate for the observational data, and therefore this model will be used to find the orbital inclination of KV UMa and the black hole mass using the wavelength range $\lambda = 6400$–$22\,000$ Å.

6 RESULTS OF MODELLING

Figs 8(a) and (b) show minimized residuals as functions of the orbital inclination i for two ratios of masses of components $q = M_{BH}/M_v = 37$ and 73 in different epochs. Horizontal dashed lines 'cut' the critical χ^2 within the significance level 1 per cent. It can be seen that in most cases minimal values of residuals are below the critical value; therefore we accept that the model 'donor star plus accretion disc with hotspot and hot line' is adequate for the observations and there is no point in rejecting it. Using minima of residuals one can find optimal values of i and corresponding parameters of the model. These values are shown in Tables 2a and b. It is evident that for $q = 37$ and 73 the optimal value of i found independently using five light curves (three optical and two

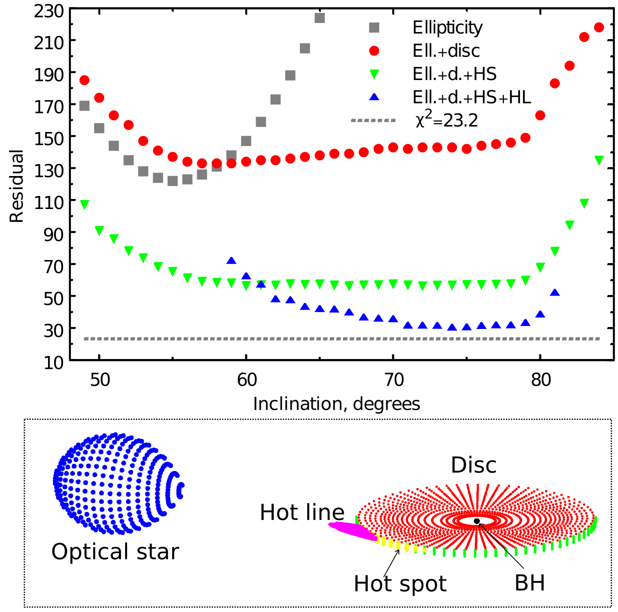

Figure 5. The adequacy test for models for the $C17$ light curve. The upper panel presents the dependences of the residual on the inclination of the orbit i that are minimal over all other parameters, $q = 37$: 'ell' is a 'purely' ellipsoidal model – there is no disc with an interaction region; 'ell+disc' is a model with an ellipsoidal donor star and a disc without a hotspot or a hot line; 'ell+disc+HS' is a model with an ellipticity effect and with a disc with a hotspot; 'ell+disc+HS+HL' is a model that includes the effect of an ellipsoidal star, an accretion disc around a black hole with a hotspot and a hot line. The horizontal line corresponds to the critical value $\chi^2_{n-m,0.01}$ within the 1 per cent confidence level. The bottom panel presents a schematic picture of the model used.

infrared) is in the ranges 68–77° and 68–79° respectively. So, the optimal value of i weakly depends on the mass ratio q. Combining the data for two values of q, we make the final estimate of the inclination of the KV UMa orbit $i = 74 \pm 4°$.

We emphasize that the value of i in our model was found without any observational information about the non-stellar component's luminosity. This luminosity in our case can be found as the solution of the inverse problem of the interpretation of the light curve (see Tables 2a and b) and can be compared with corresponding spectrophotometric estimates. Unfortunately, the scatter of observational estimates of the non-stellar component's contribution to the total luminosity of the system is significant. In addition, it seems that this contribution is different for different epochs of observations (see the introduction). Using data by Wagner et al. (2001), Zurita et al. (2002), McClintock et al. (2003), Torres et al. (2004) we can accept an average observational contribution of the non-stellar component to the total flux of the KV UMa system in the optical range (λ = 5800–6400 Å) in quiescence as 40–60 per cent. In IR in quiescence the observational estimate of the non-stellar contribution according to Mikołajewska et al. (2005), Khargharia et al. (2013) is 30–50 per cent.

The comparison of observational estimates and theoretical models (obtained from the interpretation of light curves) of the non-stellar component's luminosity $(F_{\rm d} + F_{\rm HL})/F_{\rm full})$ in the optical and IR ranges (see Tables 2a and b) shows that there is a satisfactory agreement between these estimates, and it indicates the reliability of the obtained results of modelling. Using our value $i = 74 \pm 4°$ and the mass function of the optical star $f_v(M) = 6.1 \pm 0.3\,{\rm M}_\odot$ the

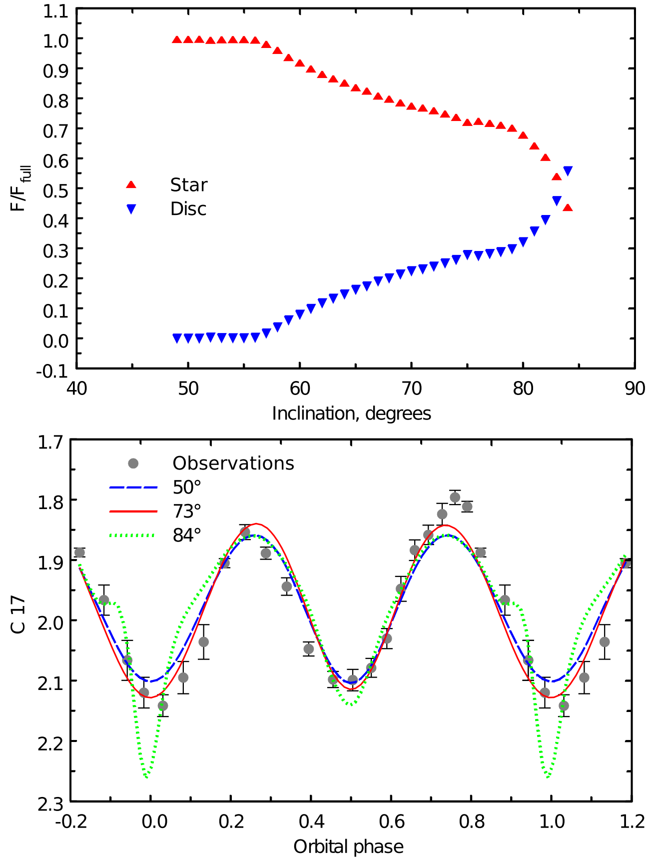

Figure 6. An output of the model 'ellipticity effect plus disc without hotspot or hot line' for the average optical light curve $C17$ (2017 November) and $q = 37$ (see Fig. 5). The upper panel shows the contribution of the star and the disc to the total system luminosity depending on the inclination i. The lower panel shows the average light curve (dots) and optimal theoretical curves for $i = 50°, 73°, 84°$. For $i = 50°$ the disc contribution is zero. For $i = 84°$ the contribution is maximal (≈55 per cent): the disc is eclipsed by the donor star.

masses of components can be found:

$$M_{\rm BH} = f_v(M)\left(1 + \frac{1}{q}\right)^2 \frac{1}{\sin^3 i};$$

$$M_v = \frac{M_{\rm BH}}{q}.$$

Using the orbit's inclination $i = 74 \pm 4°$ for $q = 37$ we found: $M_{\rm BH} = 7.24^{+0.9}_{-0.7}\,{\rm M}_\odot$, $M_v = 0.20 \pm 0.02\,{\rm M}_\odot$. For $q = 73$ and the same i the calculations gave the following results: $M_{\rm BH} = 7.06^{+0.87}_{-0.69}\,{\rm M}_\odot$, $M_v = 0.10 \pm 0.01\,{\rm M}_\odot$.

These quantities of the orbit's inclination and the black hole mass are close to estimations by Khargharia et al. (2013). The value $i = 74 \pm 4°$ obtained in the present study is consistent with the value $i = 80^{+1}_{-4}$ found by Khruzina et al. (2005) within the error limits.

6.1 Spectrum of the non-stellar component

Figs 9(a) and (b) show contributions of different components in the total luminosity of the KV UMa system for optimal model parameters for $i = 74°$ in the integral light and in bands J and K; the marks are as follows: '1' is the optical star, '2' is the accretion disc with the hotspot, '3' is the hot line. It is evident that the radiation of the tidally deformed donor star (a symmetric light curve; the star

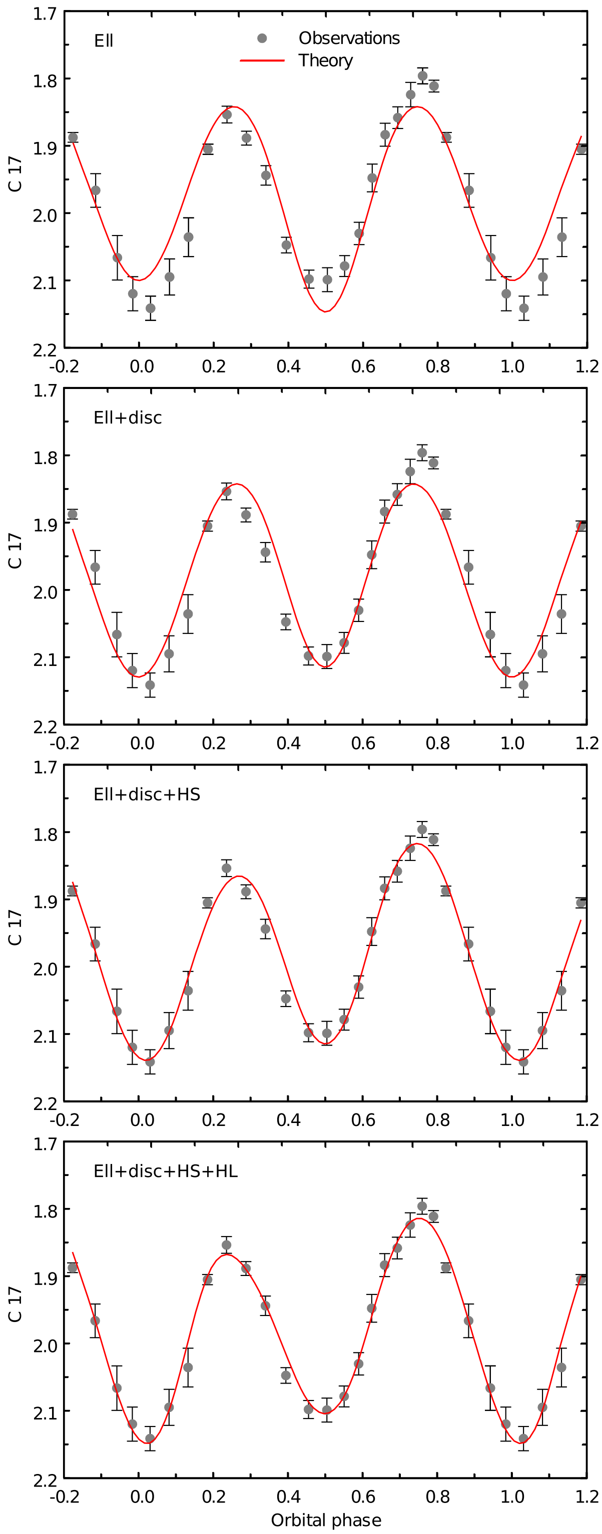

Figure 7. An illustration for residuals from Fig. 5. The average optical light curve of KV UMa (2017 November) is shown along with optimal theoretical light curves that correspond to four models of the system: 'ell' ($i = 55°$), 'ell+disc' ($i = 57°$), 'ell+disc+HS' ($i = 67°$), 'ell+disc+HS+HL' ($i = 74°$).

was warmed up with the radiation of the non-stellar component) is summarized by the radiation of the hot line, which gives a non-symmetric light curve whose contribution changes from one epoch to another. This fact explains the complicated and variable forms of the observational light curves of KV UMa. The change of the hot-line luminosity is apparently related to the change of the mass transfer rate through point L1, which strongly depends (as $\left(\frac{\Delta R}{R}\right)^3$) on the degree of overflow of the Roche lobe by the donor star, which can slightly change due to the chromospheric activity of the optical star (Cherepashchuk et al. 2019).

The dependences of the luminosities of different radiating elements averaged over the orbital period (the disc with the hotspot $F_{\rm d}$, the hot line $F_{\rm HL}$, and their sum $F_{\rm d} + F_{\rm HL}$) in units of the total luminosity of the system ($F_{\rm full}$) on the orbit's inclination i for optical and IR light curves are shown in Figs 10(a) and (b). It can be seen that in our model the luminosity of the disc with the hotspot and the luminosity of the hot line change in antiphase as functions of the orbit's inclination, so the total luminosity of the non-stellar component (the disc with the hotspot and the hot line) practically does not change with i.

Our IR light curves (see Fig. 2b) on average are 0.23^m brighter, bluer, and with a lower amplitude of the orbital variability in comparison with light curves and colours by Mikołajewska et al. (2005). The relative luminosity of the non-stellar component in them turned out to be higher in the IR than in the optical range. From Figs 10(a) and (b) it is evident that the anomalous increase of the non-stellar component's luminosity in the IR originates mostly from the increase of the luminosity of the accretion disc, and the hot line's luminosity does not show strong anomalies.

From the modelling of light curves we know the contribution of each component (the donor star, the disc with the hotspot, the hot line) to the total luminosity of the system (see Figs 9a and b). If we correct the observed average brightness taking into account the interstellar absorption (which in the case of KV UMa is very weak) and measure it in absolute energetic units we are able to find the spectrum of each component in the range λ6400–22 000 Å in absolute energetic units and restore the full spectrum of the non-stellar component (the disc with the hotspot plus the hot line). The relative contributions of each component averaged over the orbital period are shown in Tables 2a and b as functions of time (only in integral light), and as functions of the wavelength and the orbit's inclination i.

Averaged over the orbital period, stellar magnitudes of KV UMa in the $C(R)$, J and K bands (see Table 3a) were corrected taking into account the interstellar absorption. According to estimates by different authors the colour excess is small: $E_{B-V} = 0.013$–0.017 (see e.g. Hynes et al. 2000; Chaty et al. 2003). Assuming an average value $E_{B-V} = 0.015$ and following the interstellar absorption law by Rieke & Lebofsky (1985) we find the interstellar absorption $A_V = 0.046^m$ that coincides with the value $A_V = 0.05^m$ by Shahbaz et al. (2005). To calibrate the optical observations in the integral light we use the R Johnson's filter ($\lambda_{\rm eff} \approx 7000$ Å) with a central wavelength that is close to the central wavelength of the C band ($\lambda_{\rm eff} \approx 6400$ Å). To recalculate the dereddened stellar magnitudes of KV UMa averaged over the orbital period to the absolute spectral densities of fluxes F_λ we used the formula

$$F_\lambda = F_\lambda^0 \cdot 2.512^{(m_o - m)},$$

where $m_o = 0$, m is the observed stellar magnitude averaged over the orbital period (corrected accounting for interstellar absorption), F_λ^0 is the absolute spectral density of the flux of the zero stellar magnitude star outside the Earth's atmosphere.

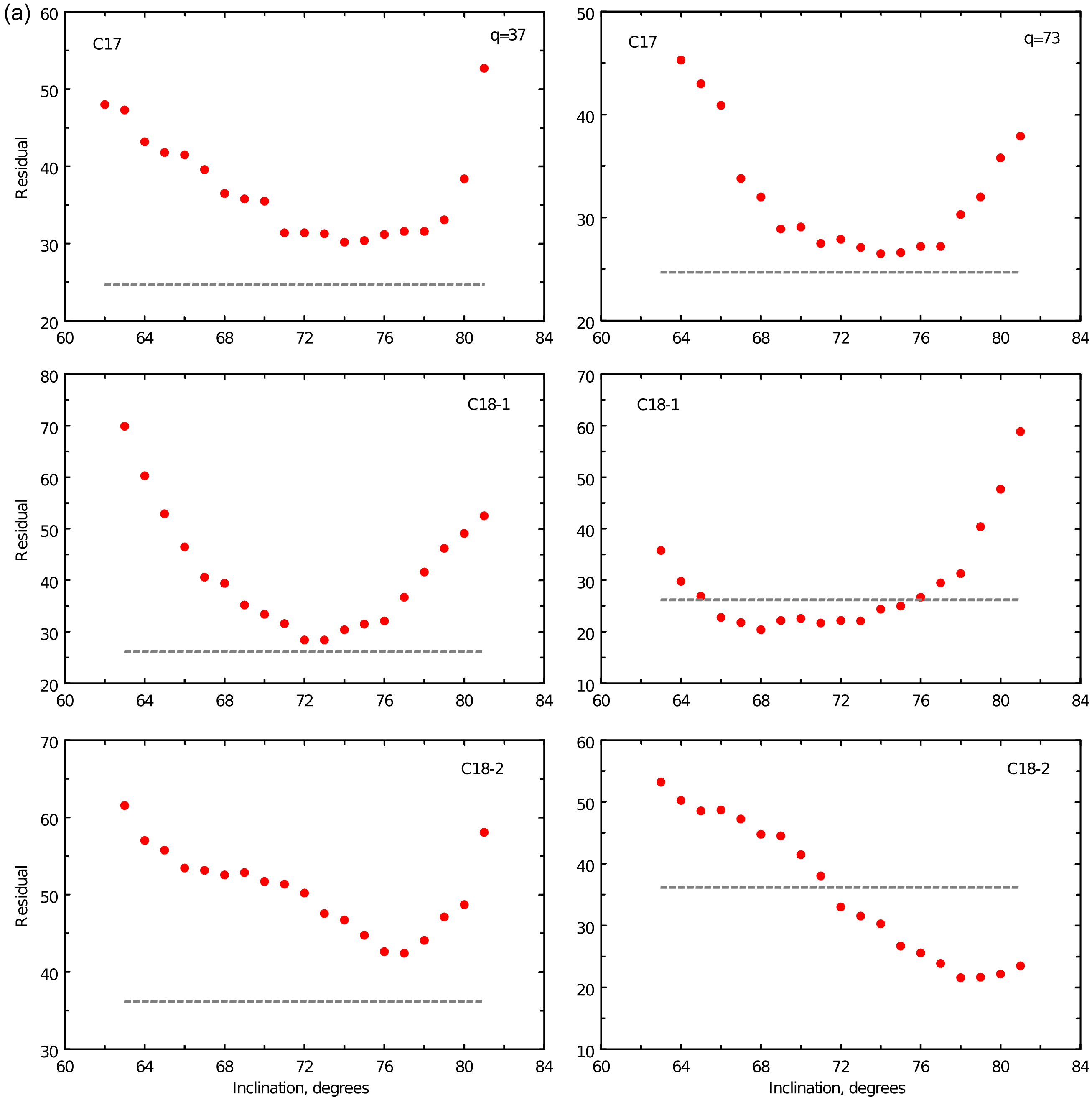

Figure 8. (a) Curves of residuals between observational and theoretical optical light curves minimized over appropriate parameters as functions of the orbit's inclination i: a horizontal dashed line 'cuts' the critical value of χ^2 within the 1 per cent confidence level (see Tables 2a and b). Curves are shown for two component mass ratios: $q = M_{\mathrm{BH}}/m_v = 37$ and 73. (b) The same as Fig. 8(a) for infrared light curves.

For the R band we used the calibration by Bessell, Castelli & Plez (1998) $F_R^0 = 2.177 \times 10^{-9}$, to find IR spectral densities of fluxes we used the calibration by Tokunaga & Vacca (2005) for MKO $F_J^0 = 3.01 \times 10^{-10}$, $F_H^0 = 1.18 \times 10^{-10}$, $F_K^0 = 4.00 \times 10^{-11}$ in units of erg cm^{-2} s^{-1} Å^{-1}. These IR calibrations are close to data by Koornneef (1983), Bessell et al. (1998).

Our average values of J, H, K stellar magnitudes were obtained over ≈130 d (from 2017 December to 2018 April); we also averaged values in the integral light over 1 yr (from 2017 November to 2018 November) neglecting average variability about 0.1^m during all optical observations. Data about the average observed stellar magnitudes and flux densities (reddened and dereddened) are shown in Tables 3a and b.

Gelino et al. (2006) calculated the *BVRJHK* distribution of the energy in the KV UMa spectrum and showed that in the B and V bands the system's flux was 65 per cent and 33 per cent higher than the flux of a K7V star, respectively. We conducted a comparison of the red end of the spectrum (*RJHK*) assuming that our flux in units $\lambda F(\lambda)$ in the J filter was equal to the flux by Gelino et al. (2006) and realized a good coincidence of them in IR (see Fig. 11). It is important to note that Gelino et al. (2006) obtained their data in 2003 January.

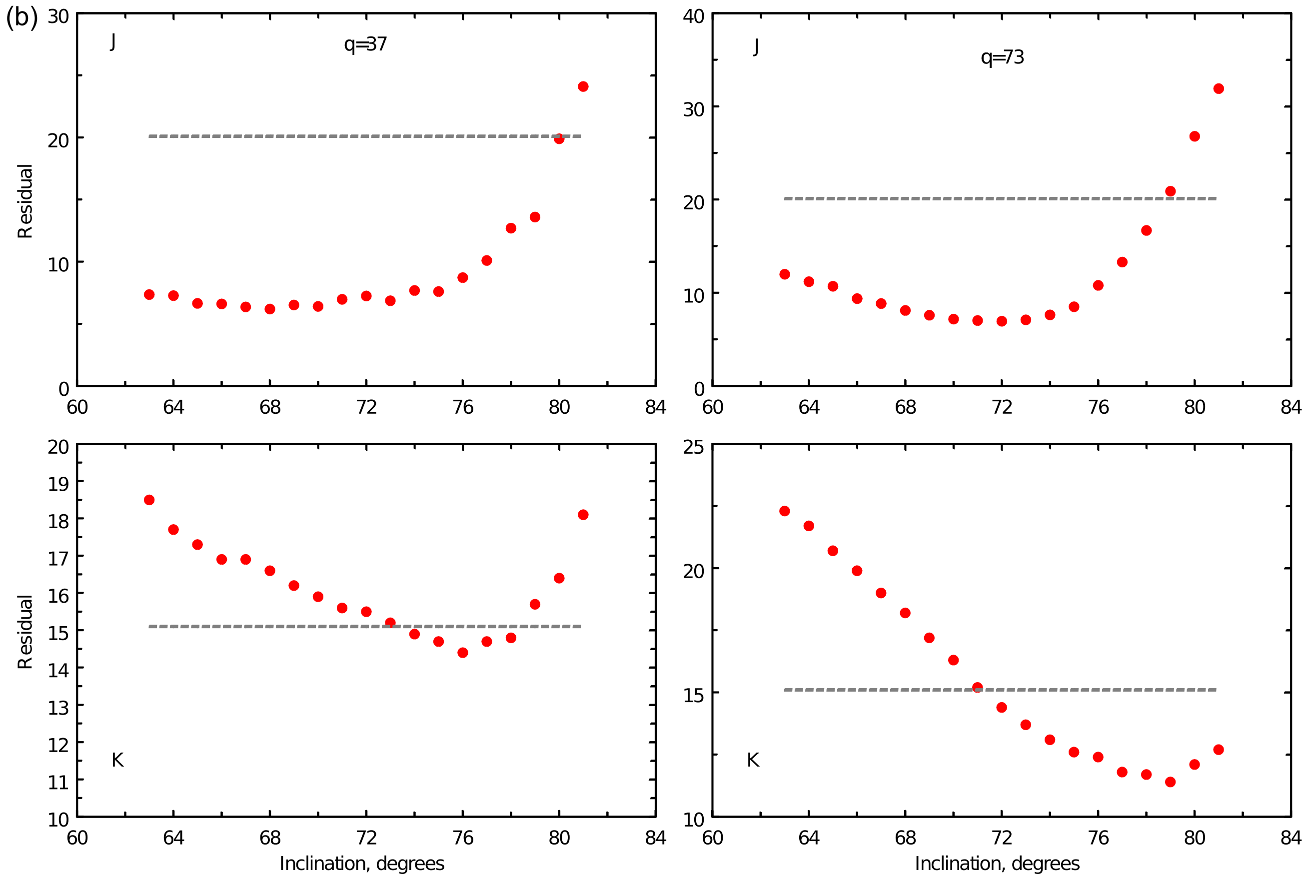

Figure 8. – *continued*

In Table 4 we collect spectral flux densities of KV UMa for $\lambda = 6400$, 12 500 and 22 000 Å averaged over the orbital period. The model flux densities are shown: $F_{\rm star}$ for the donor star, $F_{\rm d}$ for the disc with the hotspot, $F_{\rm HL}$ for the hot line, $F_{\rm d} + F_{\rm HL}$ for the whole non-stellar component. The observed flux density $F_\lambda^{\rm obs}$ is shown taking into account the interstellar absorption.

Fig. 12 shows on a logarithmic scale spectra of the non-stellar component $F_{\rm d} + F_{\rm HL}$ computed from the modelling of light curves in the $C(R)$, J, K bands for two mass ratios $q = 37$ and 73. The non-stellar component's spectrum in the range $\lambda = 6400$–22 000 Å can be fitted using a power law $F_\lambda \sim \lambda^\alpha$, where $\alpha = -1.79$ for $q = 37$ (left) and $\alpha = -1.76$ for $q = 73$ (right).

We also made analogous spectra for the accretion disc with the hotspot $F_{\rm d}(\lambda)$ excluding the hot line's contribution. The results are shown in Fig. 13. We used a fit $F_{\rm d}(\lambda) \sim \lambda^\alpha$, where $\alpha = -1.67$ for $q = 37$ (left) and $\alpha = -1.56$ for $q = 73$ (right). These results are interesting for testing models of advection-dominated accretion flows around black holes in X-ray novae in quiescence (e.g. Narayan, McClintock & Yi 1996; Esin, McClintock & Narayan 1997).

The powers in the non-stellar component's spectrum $\alpha = -1.79$ and -1.76 for KV UMa differ from the corresponding powers in the non-stellar component's spectrum of another X-ray nova A0620-00 $\alpha = -2.13$ for a passive state, but are close to $\alpha = -1.85$ for an active state (Cherepashchuk et al. 2019).

7 SEVERAL GENERALIZATIONS OF THE MODEL

We conducted an interpretation of KV UMa light curves using a comparatively simple model that has 11 free parameters. In the frame of this model we successfully gave a reliable determination of the inclination of the system's orbit, refined the masses of the black hole and of the optical star, and restored the non-stellar component's spectrum. Since there are different subtle effects in the system (chromospheric activity of the donor star, precession of the accretion disc – see the introduction) it is interesting to consider several generalizations of our model.

7.1 A model with a spotted optical star

For our optical light curve C18-2 (2018 November, $n = 30$, see Fig. 8a) the model of the close binary system in the case of $q = 37$ was inadequate. Therefore, to interpret this light curve, another model was used, a model of a system with a spotted optical star and an accretion disc without a region of interaction between the stream and the disc. As the result the quantity of variables was $m = 12$, 8 of them belonging to two 'cold' spots. In the new model the difference of maxima of the light curve can be explained by the presence of spots on the donor star. A description of the model can be found in papers by Khruzina & Cherepashchuk (1995), Cherepashchuk et al. (2019).

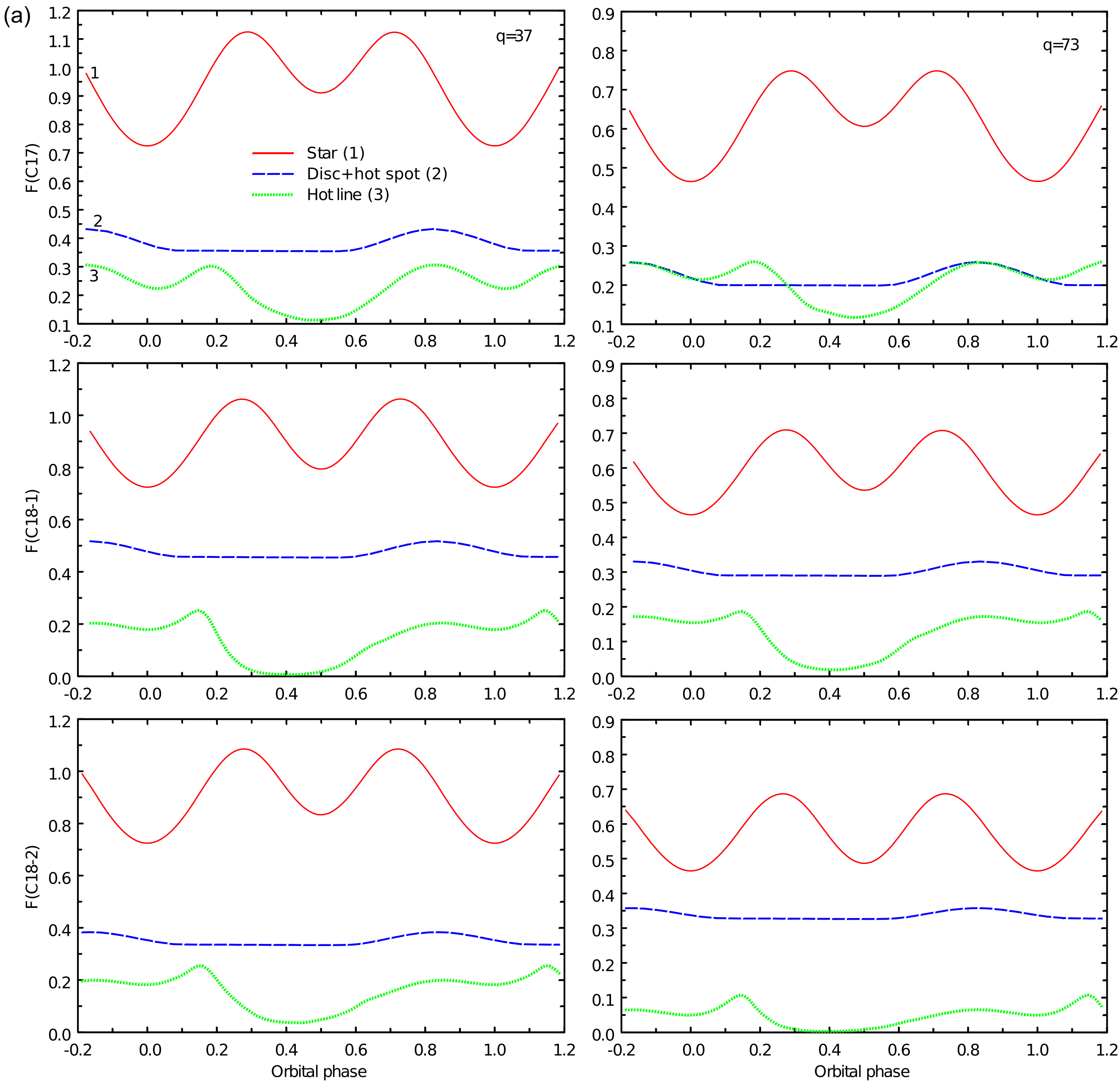

Figure 9. (a) Contributions of different components in the total luminosity of the system (in arbitrary units) for optimal parameters of the KV UMa system (see Tables 2a and b) in the integral light in 2017 (*C*17), in 2018 (*C*18-1, *C*18-2). (b) The same as Fig. 9(a) for the *J* and *K* bands.

The minimal residual in this case ($\chi^2_{\text{min}} = 55.72$) lay higher than the critical value $\chi^2 = 34.8$ within the 1 per cent significance level, i.e. the spotted model along with the hot-line model should be rejected by observations. Nevertheless, even in the frames of this not fully adequate model, we independently found a reasonable estimate of the orbit's inclination $i = 73^\circ$, which almost does not depend on the definite model of the system.

7.2 A model with a precessing accretion disc

According to spectroscopic data (Shahbaz et al. 2004; Zurita et al. 2016) in the KV UMa system there are long periodical shifts of the centroid of the H α emission line with a period of 52 d, which were interpreted as the rotation of the semi-major axis of the elliptical disc (precession) with a period that coincides with the period of superhumps on the light curves during flash attenuation (see e.g. Zurita et al. 2002). Since in our model the disc was elliptical, we tried to find from our optical light curves (which cover a time interval of 350 d) the change of the disc's orientation with time. For the search we used three optical light curves of KV UMa obtained in 2017 November, 2018 June, and 2018 November. The model with the hot line and with the elliptical accretion disc was used. The disc's orientation α_e and its eccentricity are shown in Tables 2a and b and are given for clarity in Table 5. The results depend on q weakly. The disc's eccentricity $e = 0.019$–0.025 practically did not change with time. The disc's orientation angle α_e that characterized the disc's precession was on average 125° in 2017 November, 90–95° in 2018 June, and 145–146° in 2018 November.

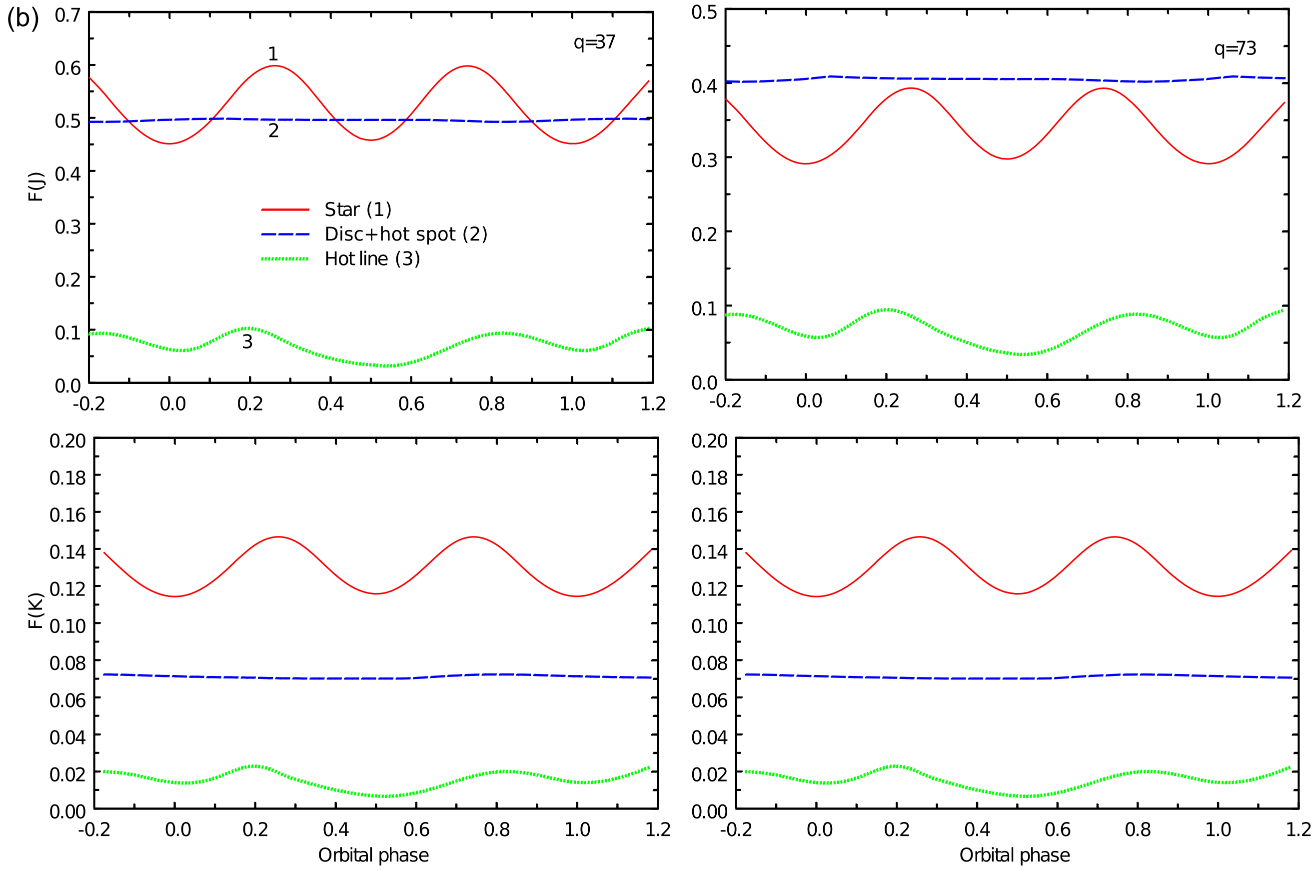

Figure 9. – *continued*

If one assumes (Shahbaz et al. 2004; Zurita et al. 2016) that $P_{\rm prec} \approx 50$–60 d, in the case of the disc's clockwise rotation, i.e. retrograde rotation according to the orbital rotation, the disc's periastron had on average 6.943 cycles over ≈348 d (341–354) from 2017 November to 2018 November; $P_{\rm prec} \approx 50.1(9)$ d. If the rotation of the disc was anticlockwise, i.e. it had the same direction as the orbital rotation, the disc made 7.057 cycles; $P_{\rm prec} \approx 49.3(9)$ d. Within error, the $P_{\rm prec}$ values for the clockwise and anticlockwise rotation were equal, so longer observational sets are needed to clarify this issue.

As follows from Table 5 the orientation angle of the disc changes from one epoch to another, so it can reflect the precession of the disc. To reliably find the disc's precession from the light curves it is necessary to obtain a dense number of observations over several months. We intend to do this in the future.

8 CONCLUSIONS

We obtained optical and IR observations of KV UMa in its quiescent state in 2017–2018 and modelled the corresponding light curves. Here we summarize the main results obtained in these studies.

(1) Our observations in 2017 November, 2018 June and 2018 November reveal no transition of the system from a passive to an active state. The system was in the passive state (using terminology by Cantrell et al. 2008) with relatively low flickering, although the average brightness of the system in the optical range over 350 d was monotonically decreasing, and in 2018 November turned out to be $\approx 0.1^m$ less than at the beginning of observations.

(2) In comparison to the J light curve obtained in 2003 and 2004 by (Mikołajewska et al. 2005), our J light curve obtained at the end of 2017 and in 2018 has an average brightness $J = 17.79^m \pm 0.02^m$ and a colour index $J - K \approx 0.73^m \pm 0.04^m$, i.e. in the IR in our case KV UMa became brighter by 0.23^m and bluer; at the same time the amplitude of variations in the J light curve dropped from 0.35^m to 0.23^m. These differences are apparently connected to the variability of the contribution of the non-stellar component: the accretion disc with the interaction region. Although the average brightness of the system was changed within wide limits, flickering in the KV UMa light curves was not detected. So, in contrast to the A0620-00 system, where the increase of the average brightness of the system is accompanied by a strong increase in flickering, in KV UMa the flickering did not appear with the increase of the average brightness of the system.

(3) We modelled optical and IR light curves of KV UMa in the frame of the model of an interacting binary system that contains a donor star filling its Roche lobe and an accretion disc with a complicated interaction region: a hot line and a hotspot. We justified the adequacy of the model with observational data.

(4) A reliable value for the inclination of the system's orbit was found ($i = 74 \pm 4°$) using the modelling of five independent light curves of KV UMa (three in the optical range and two in IR); this value is consistent with the value by Khargharia et al. (2013). Our value of i was used to find the mass of the black hole and of the donor star for two mass ratios of components: $M_{\rm BH} = 7.24^{+0.9}_{-0.7}\,{\rm M}_\odot$, $M_v = 0.20 \pm 0.02\,{\rm M}_\odot$ for $q = 37$, $M_{\rm BH} = 7.06^{+0.87}_{-0.69}\,{\rm M}_\odot$, $M_v = 0.10 \pm 0.01\,{\rm M}_\odot$ for $q = 73$. Due to the fact that $q = 73$ was found in the frame of a more developed model of the rotational broadening of

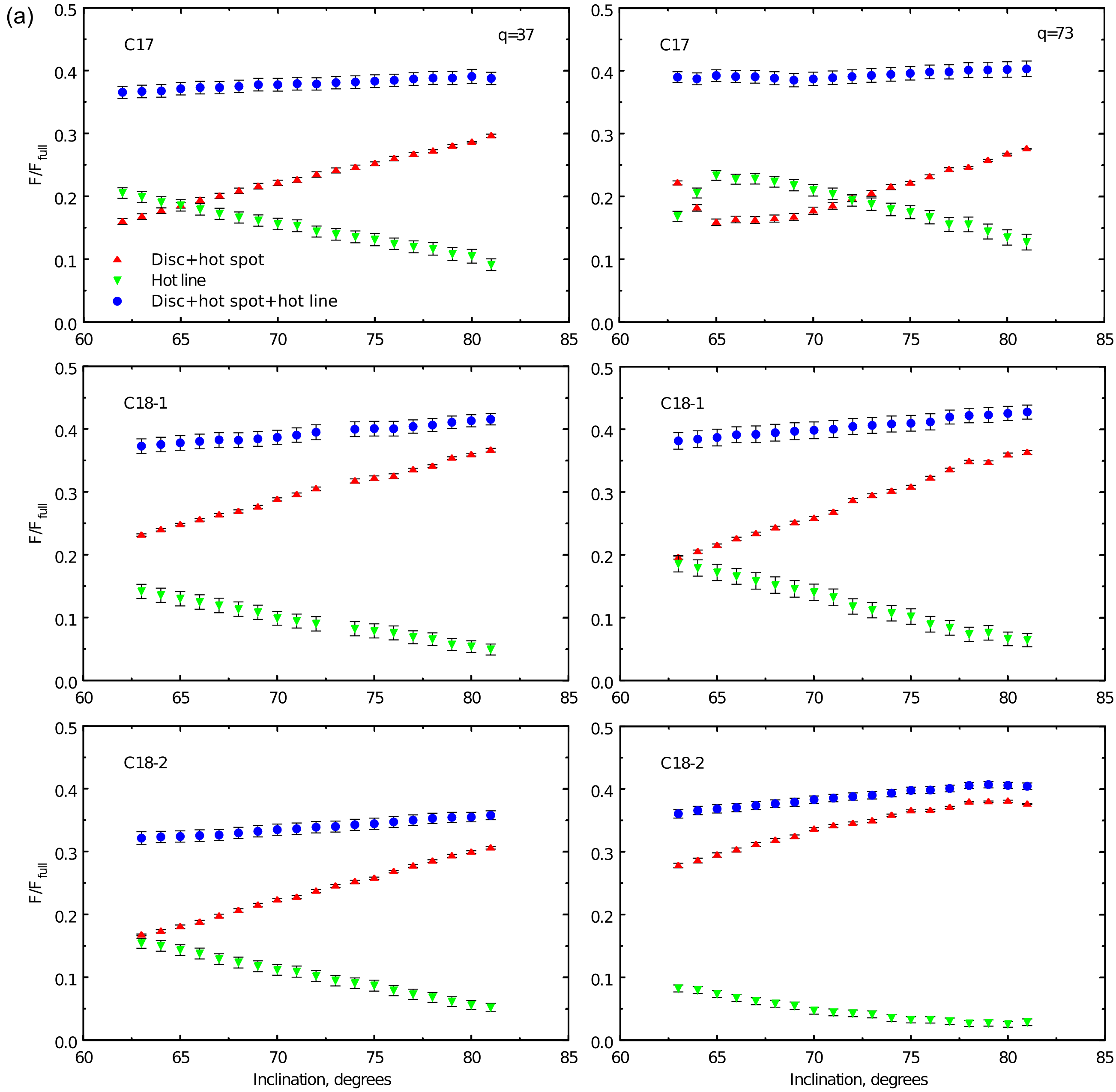

Figure 10. (a) Dependences of contributions (averaged over the orbital period) of different elements on the orbit's inclination i in the integral light (C17, C18-1, C18-2). All units are units in the total system's luminosity $F_{\rm full}$. (b) The same as Fig. 10(a) for the J and K bands.

profiles of absorption lines (Petrov et al. 2017), the masses $M_{\rm BH}$ and M_v corresponding to $q = 73$ are preferable.

(5) From the modelling of optical and IR light curves we restored the non-stellar component spectrum (the accretion disc plus the interaction region) in the range $\lambda = 6400$–$22\,000$ Å, and also the spectrum of the accretion disc (Figs 12 and 13). The non-stellar component's spectrum was satisfactory described by a power law $F_\lambda \sim \lambda^\alpha$, where $\alpha = -1.79$ for $q = 37$ and $\alpha = -1.76$ for $q = 73$. These values of α are close to values obtained for the A0620-00 X-ray nova in the active stage: $\alpha = -1.85$ (Cherepashchuk et al. 2019). The spectrum of the accretion disc can be fitted in the range $\lambda = 6400$–$22\,000$ Å by a power law $F_\lambda \sim \lambda^\alpha$, where $\alpha = -1.67$ (for $q = 37$) and $\alpha = -1.56$ (for $q = 73$); see Fig 13. These data are interesting for tests of models of advection-dominated accretion flows around black holes.

(6) We also considered two generalizations of our model and made the interpretation of optical light curves. The model with 'cold' spots on the optical star did not allow us to significantly increase the coincidence between the observed and theoretical light curves, and one of the spots was near the L1 point, potentially blocking the mass transfer between components. Therefore the model with spots on the star was not attractive. For three sets of optical observations of KV UMa (2017 November, 2018 June and 2018 November) we attempted to find traces of the precession of the elliptical accretion disc with the period 52 d found using spectrophotometric observations (Shahbaz et al. 2004; Zurita et al.

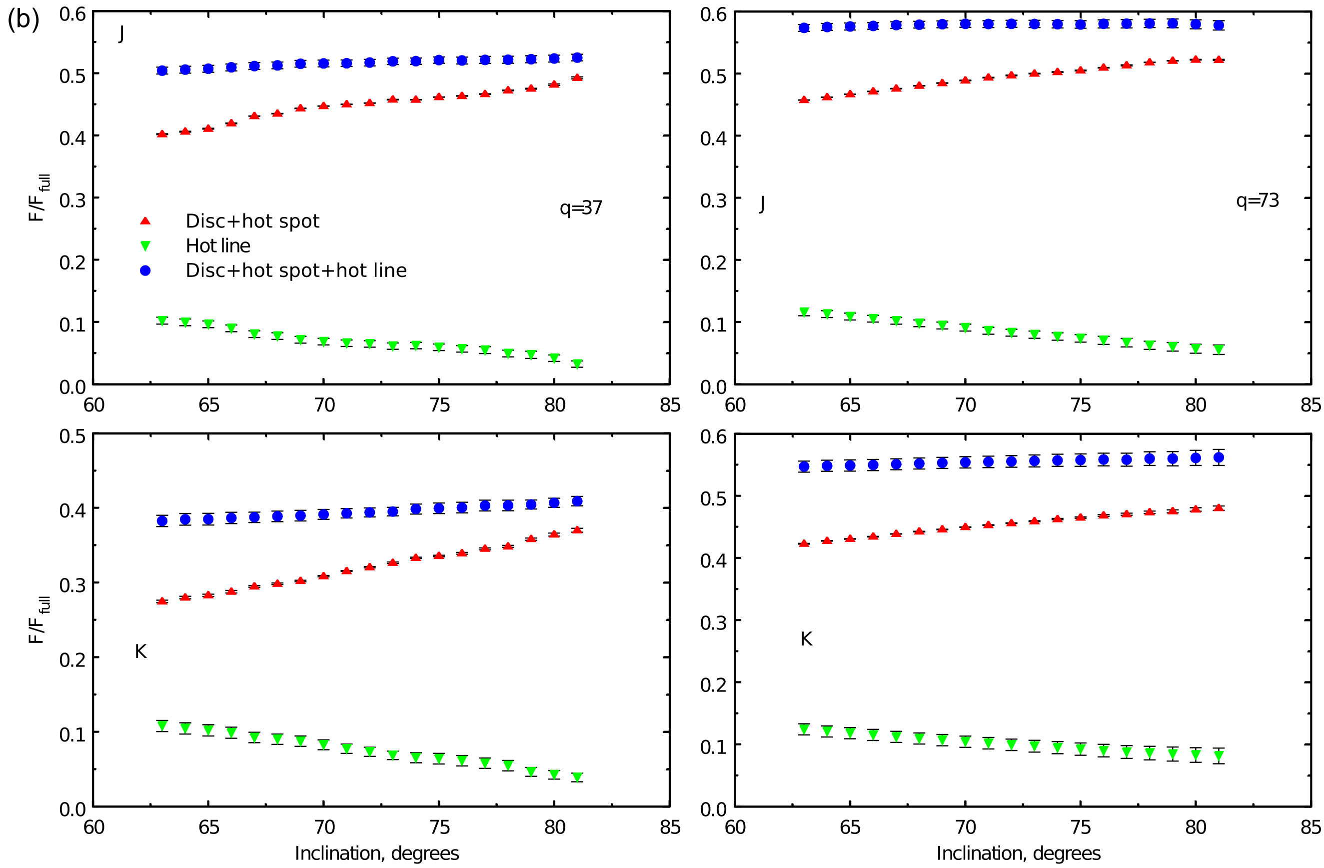

Figure 10. – *continued*

Table 3a. Average stellar magnitudes (IR magnitudes are shown in the MKO photometric system, Tokunaga & Vacca 2005).

Band	mag
R(*C*)	18.93 ± 0.01
J	17.79 ± 0.02
H	17.12 ± 0.03
K	17.06 ± 0.02

Table 3b. Spectral densities of fluxes, reddened and dereddened, in units of 10^{-17} erg cm^{-2} s^{-1} Å^{-1} (observed and accounting for the interstellar reddening).

Flux	reddened	dereddened
$F(R_C)$	5.83 ± 0.02	6.01 ± 0.02
$F(J)$	2.31 ± 0.02	2.34 ± 0.02
$F(H)$	1.67 ± 0.14	1.68 ± 0.14
$F(K)$	0.60 ± 0.01	0.60 ± 0.01

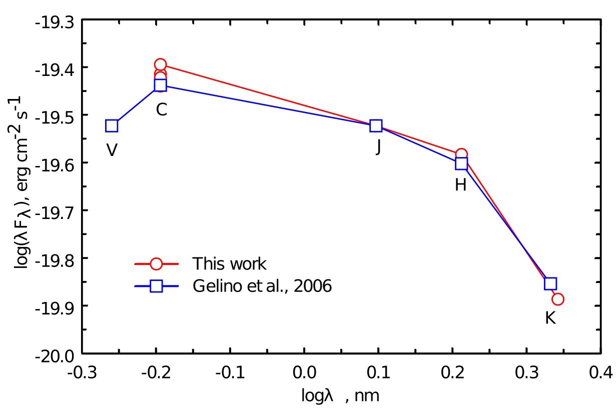

Figure 11. A comparison of the observed dereddened energy distribution in the KV UMa spectrum according to our data and according to Gelino et al. (2006); letters depict band names.

2016). The change of the disc's orientation angle from one epoch to another was detected, indicating the possibility of revealing the precession of the disc from light curves. To solve this problem it is necessary to get a dense number of light curves of KV UMa over several months; this is planned for the future.

(7) The evolutionary aspects of the problem of low-mass X-ray binary systems with anomalously rapid decrease of the orbital period are considered in the appendix. It is shown that rapid decrease of the KV UMa orbital period is consistent with the model of increased magnetic fields in the low-mass optical star during the preceding common envelope.

Table 4. Observed dereddened fluxes of KV UMa averaged over the orbital period and model fluxes in units 10^{-17} erg cm^{-2} s^{-1} Å^{-1}.

Wavelength λ, μm	$F_{\lambda\,\mathrm{obs}} = F_{\mathrm{full}}$	F_{star}	F_{d}	F_{HL}	$F_{\mathrm{d}} + F_{\mathrm{HL}}$
			$q = 37$		
0.64	6.014 ± 0.022	3.747 ± 0.126	1.672 ± 0.048	0.590 ± 0.168	2.262 ± 0.013
1.25	2.335 ± 0.024	1.137 ± 0.063	1.016 ± 0.007	0.182 ± 0.014	1.198 ± 0.012
1.63	1.679 ± 0.106	–	–	–	–
2.20	0.604 ± 0.018	0.266 ± 0.029	0.205 ± 0.006	0.037 ± 0.004	0.242 ± 0.004
			$q = 73$		
0.64	6.014 ± 0.022	3.620 ± 0.030	1.678 ± 0.054	0.716 ± 0.162	2.394 ± 0.185
1.25	2.335 ± 0.024	0.981 ± 0.024	1.160 ± 0.024	0.194 ± 0.016	1.354 ± 0.028
1.63	1.679 ± 0.106	–	–	–	–
2.20	0.604 ± 0.018	0.266 ± 0.012	0.287 ± 0.010	0.050 ± 0.008	0.337 ± 0.017

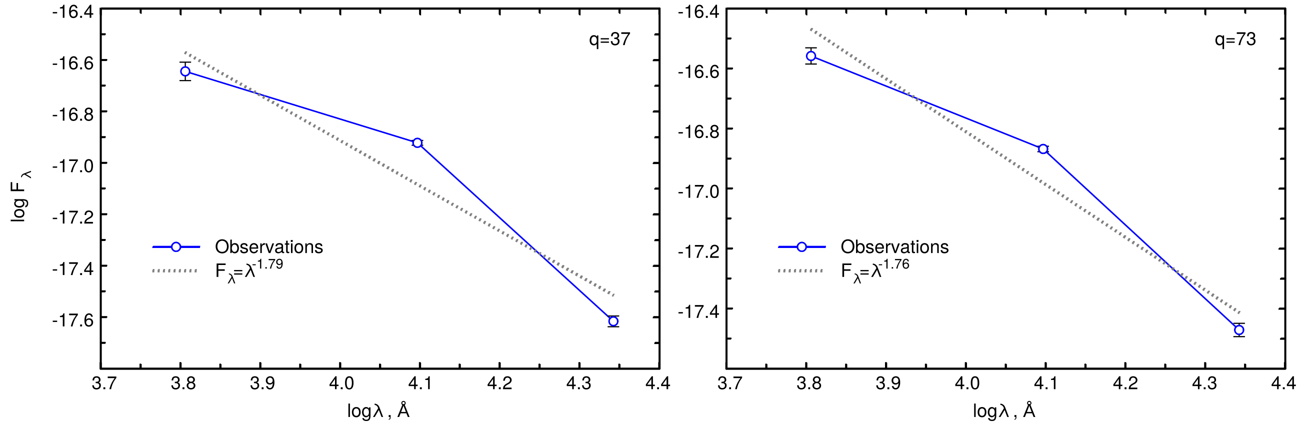

Figure 12. Spectra of the non-stellar component in the range $\lambda = 6400$–22 000 Å for $q = 37$ (left) and $q = 73$ (right).

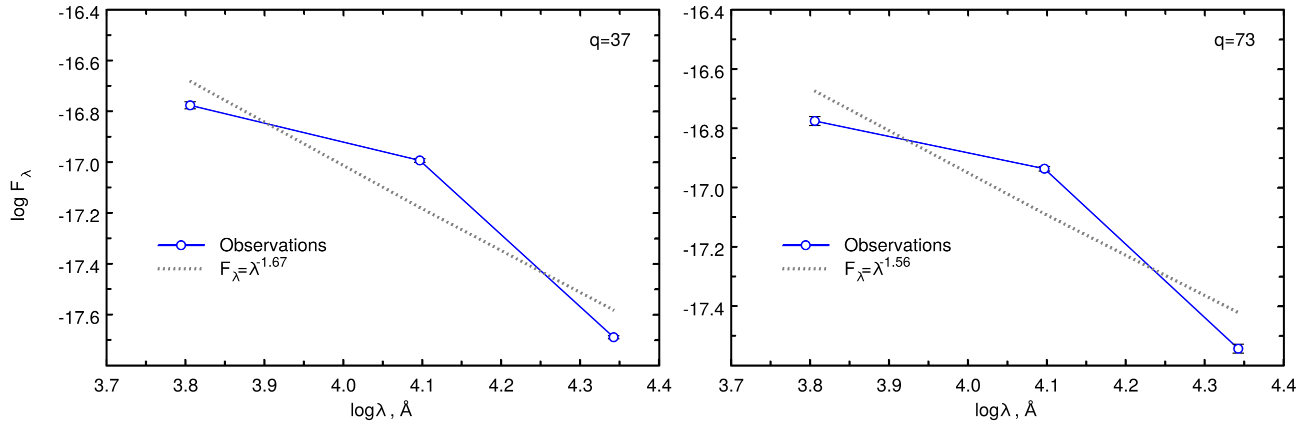

Figure 13. Spectra of the radiation of the accretion disc with the hotspot for $q = 37$ (left) and $q = 73$ (right).

Table 5. The eccentricity of the accretion disc and the angle of its orientation as functions of time.

Parameters JD 245 0000+	*C*17 8082–8083	*C*18-1 8271–8279	*C*18-2 8424–8436
		$q = 37$	
e	0.025 ± 0.004	0.019 ± 0.004	0.022 ± 0.003
α, °	125 ± 2	95 ± 2	145 ± 15
		$q = 73$	
e	0.025 ± 0.001	0.021 ± 0.004	0.022 ± 0.004
α, °	125 ± 2	90 ± 18	146 ± 5

ACKNOWLEDGEMENTS

We thank K. Atapin for his help with observations. The work of AMC (interpretation) was supported by the Russian Science Foundation grant 17-12-01241; the work of NAK, TSK, SYuS and AMT (observations and modelling) was supported by the the Program of Development of M. V. Lomonosov Moscow State University 'Leading Scientific Schools', project 'Physics of Stars, Relativistic Objects and Galaxies'. This research made use of equipment (IR camera) purchased with funds from the Program of Development of M. V. Lomonosov Moscow State University. SYuS is grateful for the APVV-15-0458 and VEGA 2/0008/17 grants of the Slovak Academy of Sciences for partial support. The authors are grateful to the anonymous referee of the manuscript for valuable comments that helped to improve it. This research has made use of NASA's Astrophysics Data System.

REFERENCES

Applegate J. H., 1992, ApJ, 385, 621
Armstrong E. et al., 2013, MNRAS, 435, 707
Arur K., Maccarone T. J., 2018, MNRAS, 474, 69
Bessell M. S., Castelli F., Plez B., 1998, A&A, 333, 231
Bisikalo D. V., 2005, Ap&SS, 296, 391
Calvelo D. E., Vrtilek S. D., Steeghs D., Torres M. A. P., Neilsen J., Filippenko A. V., González Hernández J. I., 2009, MNRAS, 399, 539
Cantrell A. G., Bailyn C. D., McClintock J. E., Orosz J. A., 2008, ApJ, 673, L159
Cantrell A. G. et al., 2010, ApJ, 710, 1127
Casares J., Jonker P. G., 2014, Space Sci. Rev., 183, 223
Casares J., Martín E. L., Charles P. A., Molaro P., Rebolo R., 1997, New Astron., 1, 299
Chaty S., Haswell C. A., Malzac J., Hynes R. I., Shrader C. R., Cui W., 2003, MNRAS, 346, 689
Chen W., Shrader C. R., Livio M., 1997, ApJ, 491, 312
Chen W.-C., Li X.-D., 2015, A&A, 583, A108
Cherepashchuk A. M., Katysheva N. A., Khruzina T. S., Shugarov S. Y., Tatarnikov A. M., Burlak M. A., Shatsky N. I., 2019, MNRAS, 483, 1067
Cook L., Patterson J., Buczynski D., Fried R., 2000, International Astronomical Union Circular, 7397, 2
Dubus G., Kim R. S. J., Menou K., Szkody P., Bowen D. V., 2001, ApJ, 553, 307
Esin A. A., McClintock J. E., Narayan R., 1997, ApJ, 489, 865
Garcia M., Brown W., Pahre M., McClintock J., Callanan P., Garnavich P., 2000, Int. Astron. Union Circular, 7392, 2
Gelino D. M., Balman, Ş., Kızıloğlu Ü., Yılmaz A., Kalemci E., Tomsick J. A., 2006, ApJ, 642, 438
González Hernández J. I., Casares J., 2010, A&A, 516, A58
González Hernández J. I., Rebolo R., Casares J., 2012, ApJ, 744, L25
González Hernández J. I., Rebolo R., Casares J., 2014, MNRAS, 438, L21
González Hernández J. I., Suárez-Andrés L., Rebolo R., Casares J., 2017, MNRAS, 465, L15
Himmelblau D. M., 1972, Applied Nonlinear Programming. McGraw-Hill, New York
Hynes R. I., Mauche C. W., Haswell C. A., Shrader C. R., Cui W., Chaty S., 2000, ApJ, 539, L37
Hynes R. I. et al., 2003, MNRAS, 345, 292
Khargharia J., Froning C. S., Robinson E. L., Gelino D. M., 2013, AJ, 145, 21
Khruzina T. S., 2011, Astron. Rep., 55, 425
Khruzina T. S., Cherepashchuk A. M., 1995, Astron. Rep., 39, 178
Khruzina T. S., Cherepashchuk A. M., Bisikalo D. V., Boyarchuk A. A., Kuznetsov O. A., 2001, Astron. Rep., 45, 538
Khruzina T. S., Cherepashchuk A. M., Bisikalo D. V., Boyarchuk A. A., Kuznetsov O. A., 2003a, Astron. Rep., 47, 214
Khruzina T. S., Cherepashchuk A. M., Bisikalo D. V., Boyarchuk A. A., Kuznetsov O. A., 2003b, Astron. Rep., 47, 848
Khruzina T. S., Cherepashchuk A. M., Bisikalo D. V., Boyarchuk A. A., Kuznetsov O. A., 2005, Astron. Rep., 49, 79
Khruzina T. S., Golysheva P. Y., Katysheva N. A., Shugarov S. Y., Shakura N. I., 2015, Astron. Rep., 59, 288
Koornneef J., 1983, A&AS, 51, 489
Kornilov V. G., Lipunov V. M., 1983, Soviet Astron., 27, 334
Lipunov V. M., Postnov K. A., Prokhorov M. E., 1996, The Scenario Machine: Binary Star Population Synthesis. Harwood, Amsterdam
Lipunov V. M., Postnov K. A., Prokhorov M. E., Bogomazov A. I., 2009, Astron. Rep., 53, 915
Lukin V. V., Malanchev K. L., Shakura N. I., Postnov K. A., Chechetkin V. M., Utrobin V. P., 2017, MNRAS, 467, 2934
Lyutyi V. M., Syunyaev R. A., Cherepashchuk A. M., 1973, Soviet Astron., 17, 1
Marsh T. R., Horne K., 1988, MNRAS, 235, 269
Masevich A. G., Tutukov A. V., 1988, Ehvolyutsiya Zvezd: Teoriya i Nablyudeniya (Evolution of Stars: Theory and Observations). Nauka, Moscow
McClintock J. E., Garcia M. R., Caldwell N., Falco E. E., Garnavich P. M., Zhao P., 2001a, ApJ, 551, L147
McClintock J. E. et al., 2001b, ApJ, 555, 477
McClintock J. E., Narayan R., Garcia M. R., Orosz J. A., Remillard R. A., Murray S. S., 2003, ApJ, 593, 435
Mikołajewska J., Rutkowski A., Gonçalves D. R., Szostek A., 2005, MNRAS, 362, L13
Nadjip A. E., Tatarnikov A. M., Toomey D. W., Shatsky N. I., Cherepashchuk A. M., Lamzin S. A., Belinski A. A., 2017, Astrophys. Bull., 72, 349
Narayan R., McClintock J. E., Yi I., 1996, ApJ, 457, 821
Ohlmann S. T., Röpke F. K., Pakmor R., Springel V., Müller E., 2016, MNRAS, 462, L121
Paczynski B., 1981, Acta Astron., 31, 1
Patterson J. et al., 2000, Int. Astron. Union Circular, 7412, 2
Pavlovskii K., Ivanova N., Belczynski K., Van K. X., 2017, MNRAS, 465, 2092
Petrov V. S., Antokhina E. A., Cherepashchuk A. M., 2017, Astron. Rep., 61, 377
Podsiadlowski P., Rappaport S., Pfahl E. D., 2002, ApJ, 565, 1107
Portegies Zwart S. F., Verbunt F., Ergma E., 1997, A&A, 321, 207
Remillard R., Morgan E., Smith D., Smith E., 2000, Int. Astron. Union Circular, 7389, 2
Rieke G. H., Lebofsky M. J., 1985, ApJ, 288, 618
Romani R. W., 1992, ApJ, 399, 621
Romani R. W., 1994, in Shafter A. W., ed., ASP Conf. Ser. Vol. 56, Interacting Binary Stars, Astron. Soc. Pac. , San Francisco, p. 196
Russell D. M., Shahbaz T., Lewis F., Gallo E., 2016, MNRAS, 463, 2680
Shahbaz T., Hynes R. I., Charles P. A., Zurita C., Casares J., Haswell C. A., Araujo-Betancor S., Powell C., 2004, MNRAS, 354, 31
Shahbaz T., Dhillon V. S., Marsh T. R., Casares J., Zurita C., Charles P. A., Haswell C. A., Hynes R. I., 2005, MNRAS, 362, 975
Shugarov S., Katysheva N., Chochol D., Gladilina N., Kalinicheva E., Dodin A., 2016, Contributions of the Astronomical Observatory Skalnate Pleso, 46, 5
Tikhonov A. N., Goncharskii A. V., Stepanov V. V., Yagola A. G., 1983, Regularizing Algorithms and A Priori Information. Nauka, Moscow [in Russian]
Tokunaga A. T., Vacca W. D., 2005, PASP, 117, 421
Torres M. A. P., Casares J., Martínez-Pais I. G., Charles P. A., 2002, MNRAS, 334, 233
Torres M. A. P., Callanan P. J., Garcia M. R., Zhao P., Laycock S., Kong A. K. H., 2004, ApJ, 612, 1026
Tutukov A. V., Kovaleva D. A., 2018, in Shustov B. M., Wiebe D. S., eds, Proc. Memorial Conf. A.G. Masevich 100th Anniversary, Stars and Satellites, Yanus-K, Moscow, p. 191

Uemura M. et al., 2000a, PASJ, 52, L15
Uemura M. et al., 2000b, Int. Astron. Union Circular, 7390, 1
Uemura M. et al., 2002, PASJ, 54, 285
van den Heuvel E. P. J., Portegies Zwart S. F., de Mink S. E., 2017, MNRAS, 471, 4256
Verbunt F., Zwaan C., 1981, A&A, 100, L7
Vilhu O., 1982, A&A, 109, 17
Wagner R. M., Foltz C. B., Shahbaz T., Casares J., Charles P. A., Starrfield S. G., Hewett P., 2001, ApJ, 556, 42
Wilson R. E., Devinney E. J., 1971, ApJ, 166, 605
Xu X.-T., Li X.-D., 2018, ApJ, 859, 46
Yungelson L. R., Lasota J. P., Nelemans G., Dubus G., van den Heuvel E. P. J., Dewi J., Portegies Zwart S., 2006, A&A, 454, 559
Zurita C. et al., 2002, MNRAS, 333, 791
Zurita C., Casares J., Shahbaz T., 2003, ApJ, 582, 369
Zurita C., González Hernández J. I., Escorza A., Casares J., 2016, MNRAS, 460, 4289

APPENDIX A: EVOLUTIONARY ASPECTS

KV UMa has an anomalous height over the galactic plane z = 1.7 kpc and shows an anomalously fast decrease of the orbital period dP/dt = -1.83 ± 0.66 ms yr^{-1} that corresponds to the change -0.85 ± 0.30 μs during one orbital cycle. This is about 150 times faster than expected from the radiation of gravitational waves by the system (González Hernández et al. 2012). González Hernández et al. (2012) suggested a model of a donor star with very strong magnetic field (>10–20 kGs) to explain so fast a decrease of the orbital period. In this case the decrease can be explained by the orbital angular momentum loss from the system by the magnetic stellar wind. The authors suggest a fast evolution of the system and a short lifetime for it. Also there is a model of an X-ray system whose anomalous fast decay of the orbital period can be explained by the interaction of the system with the circumbinary envelope (Xu & Li 2018).

It is interesting to explore the evolutionary scenario for such X-ray binaries with the SCENARIO MACHINE (a computer program for investigations into the evolution of close binary stars with the population synthesis method; Kornilov & Lipunov 1983) taking into account their short evolution time.

A1 The SCENARIO MACHINE

To study the evolution of close binary black holes with low-mass non-degenerate companions in this work the SCENARIO MACHINE was applied. With its help it is possible to study statistical properties of a population of stars as well as separate evolutionary tracks of close binary systems. The code was described in detail by Lipunov, Postnov & Prokhorov (1996), Lipunov et al. (2009); therefore here we describe only the most important free evolutionary parameters for the systems under investigation.

As the initial mass distribution function of binaries we used the Salpeter function and accepted the equiprobable initial mass ratio of components $Q = M_2/M_1 < 1$; the initial semi-major axis had a flat distribution on a logarithmic scale in the range from 10–10^6 R$_\odot$. It should also be noted that the equiprobable distribution on the initial mass ratio in the system for $Q < 0.1$ could potentially be too rough an assumption due to selection effects (Masevich & Tutukov 1988).

The rate of mass loss in the stellar wind $\dot{M}$ is essential. It can change the distance between components as well as the mass of the pre-supernova star. Also it is able to define whether the system can form a common envelope. In the case of loss of the hydrogen envelope by the progenitor of the black hole before Roche-lobe filling, the common envelope cannot form, and the X-ray nova does not form either. For main-sequence stars and supergiants we used the following formula for the mass loss:

$$\dot{M} = \frac{\alpha L}{c V_\infty} \tag{A1}$$

where L is the luminosity of the star, V_∞ is the wind's velocity at infinity, c is the speed of light and α is a free parameter. It is assumed that the full mass loss ΔM does not exceed 10 per cent of the hydrogen envelope during the lifetime in the main-sequence and supergiant stages. The mass loss by Wolf–Rayet stars was

$$\Delta M_{\rm WR} = \alpha_{\rm WR} M_{\rm WR}, \tag{A2}$$

where M_{WR} is the initial mass of the Wolf–Rayet star.

The common envelope arises if the Roche lobe is filled by the star with a highly evolved core independently of the mass ratio in the system; in other cases the common envelope forms if the condition $Q = M_2/M_1 \le q_{\rm cr} = 0.3$ is met. If $Q > 0.3$ the evolution proceeds without the common envelope (see similar conditions in recent papers by van den Heuvel, Portegies Zwart & de Mink 2017; Pavlovskii et al. 2017). For the systems under investigation this condition is always met. The common-envelope stage preceding the supernova explosion is necessary, because the current distances between the components of the systems mentioned are comparable to the size of a main-sequence star that can end its life as a black hole. The common envelope is described by the effectiveness $\alpha_{\rm CE} = \Delta E_{\rm b}/\Delta E_{\rm orb}$ (where $\Delta E_{\rm b}$ is the change in the bound energy of the envelope and $\Delta E_{\rm orb}$ is the change in the system's orbital energy); it is computed using the formula

$$\alpha_{\rm CE}\left(\frac{G M_{\rm a} M_{\rm c}}{2a_{\rm f}} - \frac{G M_{\rm a} M_{\rm d}}{2a_{\rm i}}\right) = \frac{G M_{\rm d}(M_{\rm d} - M_{\rm c})}{R_{\rm d}}, \tag{A3}$$

where $M_{\rm a}$ is the mass of the accreting star, $M_{\rm d}$ is the donor star's mass, $M_{\rm c}$ is the mass of the core of the donor star, $a_{\rm i}$ is the semi-major axis of the system at the beginning of the common-envelope stage, $a_{\rm f}$ is the semi-major axis at the end of it, and $R_{\rm d}$ is the donor star's radius.

The rate of angular momentum loss J under the influence of the magnetic stellar wind is determined by (Masevich & Tutukov 1988):

$$\frac{{\rm d}\ln J}{{\rm d}t} = -10^{-14}\frac{R_2^4 (M_1 + M_2)^2\,{\rm R}_\odot}{\lambda_{\rm MSW}^2 a^5 M_1\,{\rm M}_\odot}\,{\rm s}^{-1}, \tag{A4}$$

where R_2 and M_2 are the radius and the mass of the star with the magnetic stellar wind, M_1 is the mass of another star, a is the semi-major axis, $\lambda_{\rm MSW}$ is the parameter of the magnetic stellar wind, whose value is usually accepted to be equal to 1; in the present study it serves as a free parameter. From equation (A4) follows the time-scale of the angular momentum loss by the magnetic stellar wind (Tutukov & Kovaleva 2018):

$$\tau = \frac{3.3 a^5 M_1 \lambda_{\rm MSW}^2}{(M_1 + M_2)^2 R_2^4}; \tag{A5}$$

in this equation masses are in M$_\odot$, the semi-major axis and the radius are in R$_\odot$.

Ohlmann et al. (2016) conducted magnetohydrodynamical calculations of the common-envelope dynamics in the system consisting of a 1 M$_\odot$ main-sequence star and a 2 M$_\odot$ red giant. A common envelope in such a system may result in an increase of the magnetic field of the main-sequence star up to 10–100 kG even after 120 d from the beginning of the common-envelope stage. The increase of the magnetic field they connected with the magneto-rotational instability. Despite the masses considered by Ohlmann et al. (2016) being significantly lower than the masses of progenitors of black holes, one can accept that in a more or less similar way the accreting star's magnetic field can grow during the common-envelope stage.

In the moment of the formation of the black hole, part of the preceding star collapses under the event horizon, and part of it can be ejected. The black hole mass $M_{\rm BH}$ is calculated as

$$M_{\rm BH} = k_{\rm BH} M_{\rm preSN} \tag{A6}$$

where $M_{\rm preSN}$ is the pre-supernova mass, $0 \le k_{\rm BH} \le 1$ is a free parameter (the part of the pre-supernova star mass that falls under the event horizon). The parameter $k_{\rm BH}$ has an important value because, first, it defines the mass of the forming black hole, and, secondly, if the mass loss during the explosion exceeds 50 per cent of the total mass of stars before the supernova explosion, the system loses the gravitational bound and decays.

Also in the explosion, the star's compact remnant (a black hole) can get an additional velocity:

$$v_{\rm BH} = v_a \frac{M_{\rm preSN} - M_{\rm BH}}{M_{\rm BH}}, \tag{A7}$$

where $v_{\rm BH}$ is the additional black hole velocity and v_a is distributed as

$$f(v_a) \sim \frac{v_a^2}{v_0^3} {\rm e}^{-\frac{v_a^2}{v_0^2}}, \tag{A8}$$

where v_0 is a free parameter. The velocity's direction is equiprobable. The additional kick is important, because it can lead to the decay of the binary system, and in very particular cases it can bound systems (that should decay without it).

A2 A determination of value areas for evolutionary parameters

To find the range of valid values of the parameters $\alpha_{\rm CE}$, α, $\alpha_{\rm WR}$, $k_{\rm BH}$, v_0 we calculated the quantity of binary systems in the Galaxy taking into account their lifetimes in corresponding stages (assuming that all stars are binary). As the X-ray novae we treated a black hole paired with a low-mass non-degenerate star (with mass from 0.2–1.1 $M_\odot$) with the orbital period $\lesssim$ 0.5 d. Along with this we calculated the quantity of systems with the orbital period less than 1.5 d in order to show that the common envelope and the flat initial distribution of systems on the semi-major axis on a logarithmic scale give enough binaries with periods longer than periods of known X-ray novae, so if the magnetic stellar wind strength grows the quantity of X-ray novae remains adequate for ob servation.

According to our calculations the non-zero additional velocity of the black hole acquired during its formation $v_0 \le 10$ km s^{-1} practically does not change the quantity of the systems under investigation; the increase of v_0 over 10 km s^{-1} leads to a very rapid decrease of their quantities down to zero for $v_0 \approx 100$ km s^{-1}. Therefore the presence of X-ray novae in the Galaxy and estimations of their quantities taking into account selection effects allows us to conclude that black holes in such systems apparently do not acquire a significant kick during their formation. For this reason we use the kick velocity value $v_0 = 0$. The high distance of KV UMa from the galactic plane can probably be explained by another process (e.g. dynamical interaction with another body) or by a very specific direction of the kick and an adjusted value of it.

The rate of mass loss via the stellar wind was varied from low ($\alpha = \alpha_{\rm WR} = 0.1$) to high ($\alpha = \alpha_{\rm WR} = 0.7$). As follows from calculations,

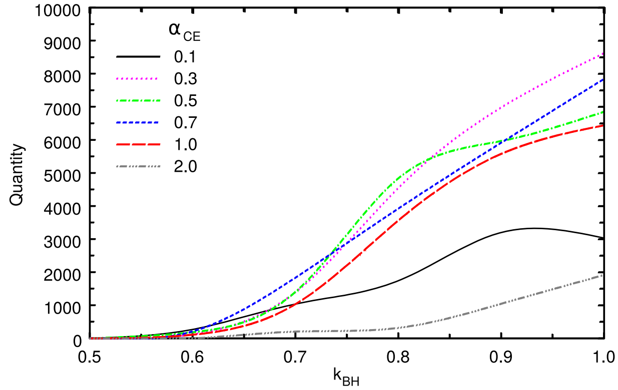

Figure A1. The number of X-ray novae in the Galaxy that consist of black holes and main-sequence stars (including those that fill their Roche lobes on the main sequence) with masses between 0.2 $R_\odot$ and 1.1 $R_\odot$. The orbital period is $P_{\rm orb} \le 0.5$ d. The following evolutionary parameters were used: $\alpha = \alpha_{\rm WR} = 0.3$, $\lambda_{\rm MSW} = 1$, $v_0 = 0$.

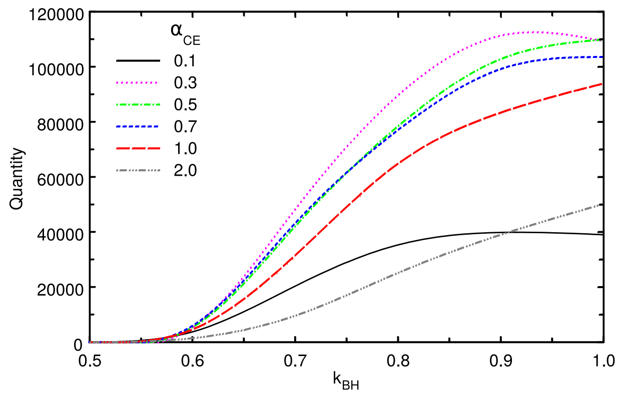

Figure A2. The same as Fig. A1 with an orbital period of $P_{\rm orb} \le 1.5$ d.

the quantity of studied systems in the Galaxy depends weakly on the strength of the wind if $\alpha \lesssim 0.5$, $\alpha_{\rm WR} \lesssim 0.5$; if the wind's strength grows further the quantity of X-ray novae rapidly falls to zero. For the calculations below we took the value $\alpha = \alpha_{\rm WR} = 0.3$ (which approximately corresponds to the solar metallicity), which allows us to make a good estimation of the quantity of systems under consideration.

Figs A1 and A2 show the quantity of studied systems calculated using different sets of evolutionary parameters; the value of $\lambda_{\rm MSW}$ was assumed to be 1. According to observational estimates the quantity of X-ray novae in the Milky Way is approximately 300–3000 (according to Chen, Shrader & Livio 1997 there are at least 100 X-ray novae with black holes; the average density of such systems is 0.25 per square kpc, which gives a rough estimate of 3000 systems in the Milky Way). A modern account for selection effects allows us to only approximately estimate the lower and upper limits of the quantity of black holes with low-mass non-degenerate stars (Arur & Maccarone 2018). This is a very soft limit that does not allow us to fix parameters. To meet the condition mentioned we chose the following set of evolutionary parameters for calculations with the modification of the strength of the magnetic stellar wind: $k_{\rm BH} = 0.8$, $\alpha_{\rm CE} = 1.0$, $\alpha = \alpha_{\rm WR} = 0.3$ (the evolutionary tracks in Tables A1, A2, and in Fig. A3 were calculated with this set too). This set allows us to get an adequate quantity of studied binaries. Also it should be noted that, in spite of the fact

Table A1. An evolutionary track that leads to the formation of a close binary system consisting of a black hole and a low-mass non-degenerate star. The magnetic stellar wind is weak ($\lambda_{MSW} = 1$). Columns in the table depict the following parameters: *System* is the composition of the binary, ΔT is the duration of the stage, M_1 is the mass of the initially more massive star, M_2 is the companion's mass ($M_{1,2}$ in $M_\odot$), a is the semi-major axis (in $R_\odot$), P_{orb} is the orbital period in days, e is the eccentricity, T is the time since the beginning of the evolution (ΔT, T in millions of years). Stages are marked as follows: 'I' is the main-sequence star, 'II' is the supergiant, '3' is the star filling its Roche lobe, 'WR' is the Wolf–Rayet star, 'BH' is the black hole, 'CE' is the common envelope. Values of evolutionary parameters are: $k_{BH} = 0.8$, $\alpha_{CE} = 1.0$, $\alpha = \alpha_{WR} = 0.3$.

System	ΔT	M_1	M_2	a	P_{orb}	e	T
I+I	4.8	31.55	0.75	750	419	0	0
I+I		28.25	0.75	830	515	0	4.8
II+I	0.48	28.25	0.75	830	515	0	4.8
II+I		19.21	0.75	1200	1079	0	5.3
3+I, CE	0.01	19.21	0.75	1200	1079	0	5.3
3+I, CE		12.55	0.75	28	4.7	0	5.3
WR+I	0.45	12.55	0.75	28	4.7	0	5.3
WR+I		8.78	0.75	39	9.15	0	5.8
		SN Ib					
BH+I	1.5E+04	7.03	0.75	50	14.7	0.23	5.8
BH+I		7.03	0.73	49	14.28	0.19	$1.5 \cdot 10^4$

Table A2. The same track as in Table A1 with a strong magnetic stellar wind ($\lambda_{MSW} = 0.13$). Values of evolutionary parameters (except λ_{MSW}), values in columns, and indicators of evolutionary stages are the same as in Table A1, 'MSW' is the stage where the evolution is strongly affected by the magnetic stellar wind, 'BB' is the Wolf–Rayet star filling its Roche lobe.

System	ΔT	M_1	M_2	a	P_{orb}	e	T
I+I	4.8	31.55	0.75	750	419	0	0
I+I		28.25	0.75	830	515	0	4.8
II+I	0.48	28.25	0.75	830	515	0	4.8
II+I		19.21	0.75	1200	1079	0	5.3
3+I, CE	0.01	19.21	0.75	1200	1079	0	5.3
3+I, CE		12.55	0.75	28	4.7	0	5.3
WR+I, MSW	0.2	12.55	0.75	28	4.7	0	5.3
WR+I, MSW		10.82	0.75	32	6.2	0	5.5
BB+3, MSW, CE	0.01	10.82	0.75	32	6.2	0	5.5
BB+3, MSW, CE		7.90	0.34	1.7	0.09	0	5.5
		SN Ib					
BH+3, MSW	30.65	6.32	0.34	2.2	0.15	0.24	5.5
MSW stage stops or the optical star decays							36.15

that low-mass X-ray binaries were mainly formed in the early stages of the evolution of the Galaxy (see fig. 2 by Yungelson et al. 2006), our conclusions do not change due to the very long lifetimes of these binaries, because the 'stockpile' of binaries in wider orbits is enough to supply the observed quantity even if there are physical reasons for a more rapid approach of components than was expected from gravitational wave radiation angular momentum losses.

A3 Calculations with variation of the magnetic stellar wind strength

Fig. A3 shows two curves; one of them depicts the quantity of studied systems with orbital periods less than 0.5 d, another curve depicts the quantity of systems with a characteristic time of angular momentum loss via the magnetic stellar wind less than 100 Myr. If the magnetic wind's strength is relatively low the second group contains no systems; with an increase in the strength the magnetic stellar wind time can become short even for systems with orbital periods longer than 0.5 d (see Fig. A2, which shows the quantity of binaries with $P_{orb} < 1.5$). It can be seen that this quantity is enough to allow the stronger wind to bring wider pairs closer, keeping the number of close X-ray novae adequate for observations. Taking into account that the quantity of X-ray novae with anomalously short time-scales of the orbital period decrease is about 15–20 per cent from all X-ray novae with measured masses of black holes, it is possible to assume that $\lambda_{MSW} \approx 0.13$ is suitable to explain the observed quantity of X-ray novae. The chosen λ_{MSW} corresponds to the increase of the angular momentum loss rate by the magnetic stellar wind by 60 times in comparison to the usual value.

Tables A1 and A2 show examples of evolutionary tracks with the same initial parameters and the same evolutionary parameters except λ_{MSW} in order to demonstrate the role of the strengthened magnetic stellar wind in the evolution. The evolution in both tracks is the same in both tables before the common envelope. Even very close approach of the stars after this stage produces no significant angular momentum loss by the magnetic stellar wind for $\lambda_{MSW} = 1$ (Table A1). In Table A2 ($\lambda_{MSW} = 0.13$) after the common envelope the secondary (low-mass) star becomes the source of the strong magnetic stellar wind that causes the strong angular momentum loss; therefore the semi-major axis grows due to the mass loss by the Wolf–Rayet star much more slowly than in the previous case.

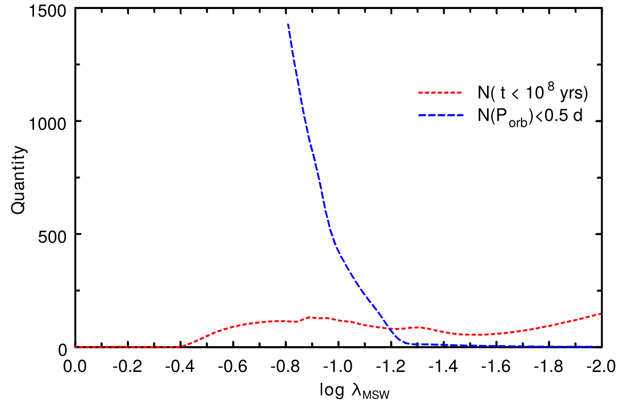

Figure A3. The quantity of X-ray novae in the Galaxy that consist of black holes and main-sequence stars (including Roche-lobe-filling stars on the main sequence) with masses between 0.2 $R_\odot$ and 1.1 $R_\odot$ depending on the magnetic stellar wind strength. The curves show the dependences of the number of binaries with an orbital period less than 0.5 d and the number of systems with a characteristic time-scale of angular momentum loss via the magnetic stellar wind less than 100 Myr (e.g. all three X-ray novae mentioned). With an increase in the rate of the angular momentum loss with the magnetic stellar wind (i.e. with the decrease of $\lambda_{\rm MSW}$) the quantity of binaries with an orbital period less than 0.5 d decreases, because the system in this range of orbital periods evolves faster and faster until the full 'sweeping' of systems from this range occurs. The quantity of systems with a characteristic time of the angular momentum loss via the magnetic stellar wind less than 100 Myr is zero if the strength of the magnetic wind is usual, and it increases to a certain amount that weakly depends on the subsequent growth of the wind's strength, because more and more wide binaries correspond to this definition. We choose the value $\lambda_{\rm MSW} = 0.13$, since in this case the ratio of the number of X-ray novae with measured masses of black holes to the number of X-ray novae with anomalously fast decreases of the orbital period approximately corresponds to observations (three binaries with a fast decrease in the orbital period among 15 X-ray novae with known masses).

This allows the Wolf–Rayet star to fill its Roche lobe, then the stars move closer to each other, and the secondary star also fills its Roche lobe, and both stars lose significant parts of their masses. After the supernova explosion, in the case of a weak magnetic stellar wind a binary system consisting of a black hole and a low-mass non-degenerate star remains; its lifetime is very long. In the case of a strong magnetic wind the formal time of the angular momentum loss according to equation (A5) becomes very short, and the fate of the system becomes unclear. If the core of a non-degenerate star is not enriched with helium at the time when the mass value becomes equal to 0.3 $M_\odot$ the magnetic stellar wind can stop (Tutukov & Kovaleva 2018); the star could lose its magnetic stellar wind when its mass drops to the mass of a brown dwarf or even a giant planet (Paczynski 1981). However, the possibility of the unlimited approach of the star to the black hole until its disintegration also remains.

A4 Conclusions from evolutionary calculations

In highly magnetized active stars the angular momentum is able to redistribute, and the star can deform. The deformation can lead to a change in the quadrupole gravitational momentum of the system (Applegate 1992). This process can cause quasi-periodical variations of the orbital period up to 10^{-5} on time-scales up to several decades. This mechanism could potentially be involved to explain the rapid approach of the components of the systems studied. Nevertheless, taking into account that all three systems with the anomalous change of the orbital period show only a decrease in the period, this is unlikely to be the main explanation.

The existence of close pairs consisting of a black hole and a very low-mass non-degenerate star means that more than half of the pre-supernova mass collapses to the black hole (otherwise the system unavoidably decays). Low or zero natal kick of the black hole during its formation is also required. Systems A0620-00 and Nova Muscae 1991 belong to the galactic disc confirming this statement. KV UMa is at a distance of more than 1 kpc from the galactic plane, which could potentially be evidence in favour of a significant natal kick for this system. If so, to keep the binarity of KV UMa the kick should have a very specific direction and a limited value (since a strong kick can disrupt the system independently of its direction). KV UMa probably got its additional velocity not in the supernova explosion process, but in dynamical interactions with other bodies.

The black hole paired with a normal star with an orbital period around several hours was most likely formed due to the common-envelope stage, because the semi-major axis of the system is less than (or very close to) the radius of the main-sequence progenitor of the black hole. In the case of X-ray novae the common envelope could be a source of strong magnetic fields in the non-degenerate star. So, angular momentum loss by the strengthened magnetic stellar wind as an explanation for the anomalous braking in the systems studied has a physical basis. To explain the observed composition and quantity of X-ray novae, an increase of angular momentum loss via the magnetic stellar wind by 60 times in comparison to the value usually used should be assumed. The value $\lambda_{\rm MSW} = 0.13$ can be slightly different if a different description is used, as, for example, in papers by Verbunt & Zwaan (1981), Vilhu (1982), Romani (1992, 1994), Portegies Zwart, Verbunt & Ergma (1997), Podsiadlowski, Rappaport & Pfahl (2002) and Yungelson et al. (2006), but the main conclusion of this evolutionary study does not change: the magnetic field of a low-mass non-degenerate star can be increased during the common-envelope stage, leading to an increased magnetic stellar wind in further evolution of the system. Nevertheless, the observed rapid approach of the components of the binaries studied could potentially have an alternative explanation, e.g. using a circumbinary disc around both components (Chen & Li 2015; Xu & Li 2018).

This paper has been typeset from a TEX/LATEX file prepared by the author.